



**FACULTY OF MECHANICAL TECHNOLOGY &  
ENGINEERING**

**SKIN FRICTION AND DIMPLE DESIGN: EXPLORING THE  
SYNERGISTIC EFFECT OF DRAG REDUCTION ON AHMED  
BODY**

**UNIVERSITY OF MALAYA  
RISSHE A/L JEYASEELAN  
B092010332**

**BACHELOR DEGREE OF AUTOMOTIVE ENGINEERING  
TECHNOLOGY (BMKA) WITH HONOURS**

**2023/2024**



## **Faculty Of Mechanical Technology & Engineering**



# **SKIN FRICTION AND DIMPLE DESIGN: EXPLORING THE SYNERGISTIC EFFECT OF DRAG REDUCTION ON AHMED BODY**

UNIVERSITI TEKNIKAL MALAYSIA MELAKA

**Rishe A/L Jeyaseelan**

**Bachelor Degree of Automotive Engineering Technology (BMKA) with Honours**

**2023/2024**

**SKIN FRICTION AND DIMPLE DESIGN: EXPLORING THE SYNERGISTIC  
EFFECT OF DRAG REDUCTION ON AHMED BODY**

**RISSHE A/L JEYASEELAN**

**A thesis submitted  
in fulfillment of the requirements for the degree of  
Bachelor Degree of Automotive Engineering Technology (BMKA) with Honors**



**UNIVERSITY OF MECHANICAL TECHNOLOGY & ENGINEERING**

**UNIVERSITI TEKNIKAL MALAYSIA MELAKA**

**2023/2024**

**BORANG PENGESAHAN STATUS LAPORAN PROJEK SARJANA MUDA**

**TAJUK: SKIN FRICTION AND DIMPLE DESIGN: EXPLORING THE SYNERGISTIC EFFECT OF DRAG REDUCTION ON AHMED BODY**

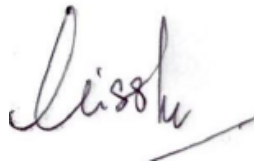
**SESI PENGAJIAN: 2023-2024 Semester 1**

Saya **RISSHE A/L JEYASEELAN**

mengaku membenarkan tesis ini disimpan di Perpustakaan Universiti Teknikal Malaysia Melaka (UTeM) dengan syarat-syarat kegunaan seperti berikut:

1. Tesis adalah hak milik Universiti Teknikal Malaysia Melaka dan penulis.
2. Perpustakaan Universiti Teknikal Malaysia Melaka dibenarkan membuat salinan untuk tujuan pengajian sahaja dengan izin penulis.
3. Perpustakaan dibenarkan membuat salinan tesis ini sebagai bahan pertukaran antara institusi pengajian tinggi.
4. **\*\*Sila tandakan (✓)**

- TERHAD** (Mengandungi maklumat yang berdarjah keselamatan atau kepentingan Malaysia sebagaimana yang termaktub dalam AKTA RAHSIA RASMI 1972)
- SULIT** (Mengandungi maklumat TERHAD yang telah ditentukan oleh organisasi/badan di mana penyelidikan dijalankan)
- TIDAK TERHAD**



Disahkan oleh:

Alamat Tetap:

**466, JALAN CENGAL 16,**  
**TAMAN CENGAL INDAH II,**  
**KULIM 09000, KEDAH.**

Cop Rasmi:



**TS. MOHD FARUQ BIN ABDUL LATIF**  
Pensyarah  
Fakulti Teknologi Dan Kejuruteraan Mekanikal  
Universiti Teknikal Malaysia Melaka (UTeM)

Tarikh: 6/2/2024

Tarikh: 6/2/2024

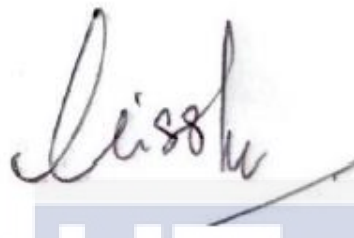
**\*\* Jika tesis ini SULIT atau TERHAD, sila lampirkan surat daripada pihak berkuasa/organisasi berkenaan dengan menyatakan sekali sebab dan tempoh laporan PSM ini perlu dikelaskan sebagai SULIT atau TERHAD.**

## DECLARATION

I declare that this Choose an item. entitled “Skin Friction and Dimple Design: Exploring the Synergistic Effect of Drag Reduction on Ahmed Body” is the result of my own research except as cited in the references. The Choose an item. has not been accepted for any degree and is not concurrently submitted in candidature of any other degree.

Signature

:



Name

:

RISSHE A/L JEYASEELAN

Date

:

11/01/2024



اونيورسيتي تيكنيكل مليسيا ملاك

UNIVERSITI TEKNIKAL MALAYSIA MELAKA

## APPROVAL

I hereby declare that I have checked this thesis and, in my opinion, this thesis is adequate in terms of scope and quality for the award of the Bachelor of Mechanical Engineering Technology (Automotive Technology) with Honors.

  
TS. MOHD FARUQ BIN ABDUL LATIF  
Pensyarah  
Fakulti Teknologi Dan Kejuruteraan Mekanikal  
Universiti Teknikal Malaysia Melaka (UTeM)

Signature :

Supervisor Name : *MOHD FARUQ BIN ABDUL LATIF*

Date : 06/02/2024



## DEDICATION

This project and research work is dedicated to my beloved parents for their enthusiastic caring throughout my life, my loving sibling and also my friends for their encouragement and love. To my supervisor, Mr. Mohd Faruq Bin Abdul Latif, lecturers and friends for all of their help.



## ABSTRACT

Buses play a vital role in public transportation today. However, due to their large size, they experience significant aerodynamic drag when traveling at high speeds over long distances. This research aims to optimize the reduction of drag coefficient by introducing dimples on the top surface of an Ahmed Body, using Skin Friction approaches. The primary cause of this drag is the inefficient aerodynamic shape, resulting in the separation of the boundary layer. In particular, the separation occurring at the top of the bus contributes significantly to the high drag coefficient and skin friction. To address this issue, the Ahmed Body, a simple 3D bluff body representing a simplified car, was selected for simulation in this research (Beaudoin & Aider, 2008). A modified Ahmed Body model, resembling the actual bus geometry, was developed, and a virtual wind tunnel test was conducted to determine the benchmark drag coefficient. To mitigate the problem, the implementation of dimples on the vehicle's roof was proposed as a solution. These dimples serve to delay boundary layer separation and reduce skin friction, resulting in a lower drag coefficient. The effectiveness of this approach was evaluated through simulations using the Virtual Wind Tunnel in Ansys Fluent. Additionally, a comprehensive analysis was performed to thoroughly investigate the relationship between the drag coefficient and skin friction.

UNIVERSITI TEKNIKAL MALAYSIA MELAKA



## **ABSTRAK**

*Bas merupakan salah satu pengangkutan awam penting pada zaman ini. Saiz besar bas menyebabkan ia mengalami rintangan aerodinamik yang besar apabila bergerak pada jarak jauh dengan kelajuan tinggi. Objektif kajian ini adalah untuk mengoptimumkan pengenalan lubang-lubang kecil pada permukaan atas Badan Ahmed bagi mengurangkan pekali rintangan menggunakan pendekatan Geseran Kulit. Ini disebabkan oleh bentuk aerodinamik yang tidak cekap, menyebabkan lapisan sempadan berasingan. Khususnya, perasingan yang berlaku di bahagian atas bas memberikan sumbangan yang besar kepada pekali rintangan yang tinggi dan geseran kulit. Pertama, reka bentuk geometri yang dipanggil Badan Ahmed dipilih untuk disimulasikan dalam kajian ini kerana ia merupakan badan tebing 3D yang mudah, mewakili kereta yang sangat dipermudahkan (Beaudoin & Aider, 2008). Satu model rujukan Badan Ahmed dengan beberapa perubahan sudut condong belakang dibangunkan bagi mewakili geometri sebenar bas dan disimulasikan dalam ujian terowong angin maya untuk mendapatkan pekali rintangan rujukan. Bagi menangani isu ini, satu penyelesaian yang melibatkan pelaksanaan lubang-lubang kecil pada bumbung kenderaan telah dicadangkan. Lubang-lubang kecil ini berfungsi untuk melambatkan perasingan lapisan sempadan dan mengurangkan geseran kulit, akhirnya mengurangkan pekali rintangan. Untuk menilai keberkesanan pendekatan ini, simulasi dilakukan menggunakan Terowong Angin Maya dalam aliran Ansys Fluent. Selain itu, analisis menyeluruh dijalankan untuk menyiasat hubungan antara pekali rintangan dan geseran kulit.*

## ACKNOWLEDGEMENTS

I would like to express my heartfelt dedication of my dissertation work to my beloved family and friends. Their unwavering support and encouragement have been instrumental throughout this research journey.

I am immensely grateful to my supervisor, Mr. Mohd Faruq Bin Abdul Latif, whose invaluable guidance and mentorship played a pivotal role in the successful completion of this project. His expertise and unwavering support significantly contributed to the smooth progression of my research.

I extend my deepest gratitude to my mother, Mrs. Prema A/P Raman Kutty, as well as my entire family. Their constant encouragement and belief in my abilities were instrumental in providing the motivation to see this project through to its completion.

Lastly, I would like to extend my sincere appreciation to the Faculty of Engineering Technology (FTKM) at UTeM, all the lecturers, and my friends who have directly or indirectly supported me during my Final Year Project. The cooperative support and camaraderie from these individuals have been invaluable in shaping the outcome of my research.

## TABLE OF CONTENTS

	<b>PAGE</b>
<b>DECLARATION</b>	
<b>APPROVAL</b>	
<b>DEDICATION</b>	
<b>ABSTRACT</b>	<b>i</b>
<b>ABSTRAK</b>	<b>ii</b>
<b>ACKNOWLEDGEMENTS</b>	<b>iii</b>
<b>TABLE OF CONTENTS</b>	<b>iv</b>
<b>LIST OF TABLES</b>	<b>vi</b>
<b>LIST OF FIGURES</b>	<b>vii</b>
<b>LIST OF SYMBOLS AND ABBREVIATIONS</b>	<b>ix</b>
<b>LIST OF APPENDICES</b>	<b>x</b>
<b>CHAPTER 1 INTRODUCTION</b>	<b>1</b>
1.1 Background	1
1.2 Problem Statement	4
1.3 Research Objective	5
1.4 Scope of Research	5
<b>CHAPTER 2 LITERATURE REVIEW</b>	<b>6</b>
2.1 Introduction	6
2.1.1 Identification Method	7
2.1.2 Screening Method	8
2.1.3 Eligibility Method	9
2.1.4 Inclusion Method	11
2.2 Outcome of SLR	12
2.2.1 Table Author & Findings	13
2.3 Design	24
2.4 Modelling	40
2.5 Skin Friction	46
2.5.1 Introduction	46
2.6 Terminology of Skin Friction	48
2.7 CFD and Altair	50
2.8 Reynolds Number	51
2.9 Fuel Consumption	53

<b>CHAPTER 3</b>	<b>METHODOLOGY</b>	<b>55</b>
3.1	Introduction	55
3.2	Flowchart	56
3.3	Pre-processing	58
	3.3.1 Modeling	59
	3.3.2 Meshing	60
	3.3.3 Boundary Condition and CFD	62
3.4	Computational Domain	64
3.5	Post Processing	67
3.6	Results	70
<b>CHAPTER 4</b>	<b>RESULTS AND DISCUSSION</b>	<b>71</b>
4.1	Introduction	71
4.2	Ahmed body model	71
4.2.1	Benchmark drawing of Ahmed Body	72
4.2.2	Drag reduction device (Dimple Plate) on Ahmed Body	73
4.2.3	Meshing	74
4.3	Ansys CFD Fluent Flow	76
4.3.1	Mesh and Ansys for 3 million dimple plate	78
4.4	Benchmark vs Dimple plate (Bluff Body)	80
4.4.1.	Pressure Plot on Middle Surface	80
4.4.2.	Coefficient Drag	81
4.4.3.	Coefficient Lift	82
4.4.4.	Coefficient Moment	83
4.4.5.	Skin Friction Acting upon surface	84
<b>CHAPTER 5</b>		<b>85</b>
5.1	Introduction	85
5.2	Conclusion	85
5.3	Impact Research	86
5.4	Recommendations of future work	86
<b>REFERENCE</b>		<b>87</b>

## LIST OF TABLES

TABLE	TITLE	PAGE
Table 2.1	Author and findings according to year published	13
Table 2.1	Comparison between the experiment data and simulated 35 Ahmed model.	40
Table 2.2	Comparison of standard 25 Ahmed model with Top_big_20 and Top_small_40.	41
Table 3.1	Analysis setup	66
Table 4.1:	Mesh sizes	74
Table 4.1:	Boundary Conditions	76



## LIST OF FIGURES

FIGURE	TITLE	PAGE
Figure 2.1	Flow of information through the different phase of systematic review	12
Figure 2.2	Experimental Investigation of Flow Control over an Ahmed Body using DBD Plasma Actuator,	25
Figure 2.3	Ahmed body dimensions	26
Figure 2.4	: Ansys view of Ahmed model	27
Figure 2.5	: Fluctuating Headwind Conditions	28
Figure 2.6	: Compressible Laminar Boundary-Layer Flows	32
Figure 2.7	: Ahmed body in varying flow conditions	35
Figure 2.8	: longitudinal vortices on a fat back Ahmed body	39
Figure 2.9	: Mesh Details (Du et al., 2019)	45
Figure 3.1	: Example of meshing on Ahmed body (Khan & Umale 2014) Then after finished meshing process quality index will be made to ensure the meshing is good to go simulation process. Another objective of this quality index is to evaluate the capability of the under-lying meshing scheme regarding thin gaps in complex models (Gnech & Ratzel 2012)	61
Figure 3.2	: The Dimensions Of The Wind Tunnel	62
Figure 3.3	: The size of wind tunnel	65
Figure 3.4	: Front view Of wind tunnel	65
Figure 3.5	: The refinement zone placement	65
Figure 4.1	; represent a benchmark model	72
Figure 4.2	: The dimension of Model with Drag reduction device (Dimple Plate)	73

Figure 4.4	: The mesh of benchmark bluff body (800k – 5million)	75
Figure 4.5	: calculation of velocity	76
Figure 4.6	: pressure plot 800k to 5 million	77
Figure 4.7	: Mesh view for dimple plate design	78
Figure 4.8	: Pressure Plot Dimple Plated Bluff Body	79
Figure 4.8	: Pressure Plot Benchmark vs Dimple Plate (bluff body)	80
Figure 4.9	: Coefficient Drag comparison graph	81
Figure 4.11	: Coefficient Lift comparison graph	82
Figure 4.12	: Coefficient Moment comparison graph	83
Figure 4.13	: Skin Friction on surface (Benchmark vs Dimple Plate)	84







## LIST OF SYMBOLS AND ABBREVIATIONS

-  
-  
-  
-  
-  
-  
-  
-



# CHAPTER 1

## INTRODUCTION

### 1.1 Background

The imperative to decrease global vehicle fuel consumption in order to effectively address climate change is both critical and urgent. A key aspect of this effort lies in the research and development of methods to reduce aerodynamic drag, thereby enhancing fuel efficiency. This undertaking holds significant environmental implications. To accomplish substantial reductions in aerodynamic drag, it is imperative to gain a thorough understanding of the flow dynamics surrounding vehicles. As noted by Hucho and Sovran in 1993, this comprehensive understanding is crucial for achieving effective drag reduction and optimizing the overall sustainability of vehicles. This introduction sets the stage for the university project, emphasizing the significance of investigating and implementing measures to enhance fuel efficiency in the context of mitigating climate change.

To facilitate the study and validation of various aspects of a vehicle, it was recognized that employing a simplified generic model would be more practical, given the complexity of aerodynamics in an actual vehicle. As a result, several generic vehicle models were developed, and one extensively investigated model is the Ahmed body, as documented by Ahmed et al. in 1984. Recent research has shed light on the correlation between base drag and the recirculation region formed at the rear of a bluff body. In the case of an axisymmetric bluff body, it has been observed that

an increased thickness of the boundary layer prior to separation leads to a reduction in base pressure. This alteration in the flow's incipient instability shifts the recirculation region downstream and extends its length, as indicated by studies conducted by Mariotti, Buresti, Salvetti (2015) and Mariotti, Buresti (2013). The introduction of this university project highlights the rationale behind utilizing a simplified generic model, specifically the Ahmed body, to investigate and comprehend the intricacies of base drag and the recirculation region, ultimately contributing to the broader understanding of vehicle aerodynamics.

Despite their numerous advantages, buses also face certain drawbacks, one of which is their substantial frontal area. This characteristic significantly contributes to an increased drag coefficient, resulting in higher resistance to airflow. As air passes over a solid surface, a thin boundary layer forms between the primary air stream and the surface. Separation of this boundary layer leads to a heightened drag coefficient. Therefore, reducing drag becomes crucial as it directly influences fuel economy. This observation, as highlighted by Gopal and Senthilkumar in 2013, underscores the importance of investigating methods to mitigate drag and enhance fuel efficiency in the context of bus design and operation. This introduction sets the context for the university project, emphasizing the significance of addressing drag reduction to achieve improved fuel economy for buses.

The objective of this research project is to investigate the application of a dimple structure on the front section of a bus. Dimples, known for their use in golf balls to delay boundary layer separation and reduce drag coefficient, will be employed in this study. To achieve this, CATIA software will be utilized to design the dimple on a drag reduction product to be attached to the top of the Ahmed body.

Additionally, Computational Fluid Dynamics (CFD) software will be utilized to simulate the external airflow around the modified bus model. The research conducted by Yamin in 2016 has already explored the analysis of external airflow on buses using CFD simulation. Notably, the results of Yamin's study have demonstrated that steady-state CFD simulations can effectively contribute to the aerodynamic optimization of bus designs. By building upon this prior research, this university project aims to further investigate and enhance the aerodynamic performance of buses through the integration of dimple structures and advanced simulation techniques.



## 1.2 Problem Statement

The aerodynamic drag encountered by heavy vehicles, notably trucks and buses, is reaching an alarming level of significance that cannot be disregarded. Their substantial frontal area and suboptimal aerodynamic profiles contribute to elevated drag coefficients and subsequent fuel consumption, compromising efficiency (Altaf et al., 2014). In the dynamic landscape of the contemporary global economy, the management of vehicle aerodynamic drag has emerged as a preeminent research problem in the field of vehicle aerodynamics, with far-reaching implications for the fuel efficiency of numerous automobile models (Hanfeng et al., 2016; Martin-Alcàntara et al., 2014). Therefore, it is imperative to explore strategies aimed at reducing the drag coefficient to unlock the potential for enhanced vehicle efficiency (Sharma et al., 2015).

Understanding the intricate interplay between pressure drag and friction drag is crucial in comprehending the phenomenon of aerodynamic drag. The geometry of a vehicle significantly influences pressure drag, which occurs due to the separation of the boundary layer at the rear trailing end, leading to the formation of a wake region behind the vehicle (Sharma et al., 2015). In the case of bluff bodies, effective drag reduction entails skillfully managing or modifying the flow patterns surrounding the body (Altaf et al., 2014). Recent research has centered on investigating various techniques for reducing aerodynamic drag in the Ahmed body model. These approaches involve employing vortex generators positioned on the model's roof (Aider et al., 2010; Pujals et al., 2010), implementing deflectors at the edges of the slanted surface and vertical base (Beaudoin and Adler, 2018; Fourrie et al., 2011), and applying steady suction at the top edge of the slanted surface (Roumeas et al., 2008).

### 1.3 Research Objective

The objectives are as follows:

- To design and develop an effective drag reduction device for enhancing the aerodynamic performance of Ahmed body.
- To assess and evaluate the effectiveness of the developed drag reduction device in improving the aerodynamic performance of Ahmed body.
- To analyze and investigate the impact of flow on skin friction in order to gain a better understanding of its effects on the aerodynamic performance of Ahmedbody.

### 1.4 Scope of Research

The scope of this research are as follows:

- The dimple shape optimization technique was implemented on the upper surface of the Ahmed body.
- Minimizing the drag coefficient and skin friction experienced by an Ahmed body.
- The size of the dimples was determined through an analysis of the drag coefficient and skin friction, employing Hyperworks and Computational Fluid Dynamics (CFD) in Ansys.
- The primary focus of this study centers on the boundary layer situated at the upper region.
- The design of the drag reduction device incorporating dimples was created using Catia.

## CHAPTER 2

### LITERATURE REVIEW

#### 2.1 Introduction

The PRISMA (Preferred Reporting Items for Systematic Reviews and Meta-Analyses) method is a well-established tool for conducting systematic reviews in the field of literature review. The PRISMA method stands out as an exceptional resource for guiding research efforts toward optimal outcomes. (Moher et al., 2010).

Thanks to this incredibly detailed approach that includes searching numerous databases/sources (even those with obscure or niche information), grey literature is no longer left out of consideration when trying to identify materials pertinent to one's topic at hand. Once identified articles/studies have been gathered using multi-faceted approach inclusive of both online/offline searches they receive rigorous scrutiny based upon several key factors including: Study designs/Pub date/Language availability - ultimately establishing rigorously vetted research material that meets pre-determined standards reflecting qualitative methodology/practices. (Page & Moher, 2017).

A comprehensive literature review can be accomplished by employing either quantitative meta-analyses or narrative syntheses techniques. The ensuing results are accurately communicated through graphical representations such as tables alongside supporting explanatory text. Ultimately, the PRISMA approach provides rigorous in consistency throughout the process of conduction of such research reviews. (Page & Moher, 2017).

### 2.1.1 Identification Method

As part of its methodology for conducting a robust literature review process, the PRISMA approach emphasizes critical steps such as the identification phase which is pivotal in determining relevant research work to include in analysis. In achieving this goal efficiently through comprehensive searches across various databases such as Scopus or Web of science etc., optimization strategies may be needed while also considering grey-literature and referencing lists from related works as suggested by PRISMA guidelines. (Moher et al., 2010)

Typically, there are two stages of this process where the study is screened for eligibility based on inclusion and exclusion criteria. In this case, the website used to search Web Of Science and Scopus where we used the keywords of "AHMED BODY" AND "DRAG" instead of adding sin friction to the search due to less research done on the topic and not within the 5 years range which is from 2019 to 2023. (Moher et al., 2010)

From the search web Scopus, we gained around 272 articles that were related to the topic or keywords inserted. While from the Web of Science (WOS), a total of 170 researches shown as a result where when the researches were combined together in the Mendeley software, there were around 12 articles were found to be duplicate or similar and removed from the total which concludes around 430 researches. (Page & Moher, 2017).



### 2.1.2 Screening Method

Screening is a method used to quickly identify relevant information from a large pool of data. In research, screening involves reviewing titles and abstracts of articles to determine their potential relevance. To maintain high standards, a team of two or more independent reviewers generally assesses studies and selects only those that fulfil the inclusion criteria for subsequent analysis. Any inconsistencies are settled through dialogue or consulting with an additional reviewer. (Liberati, 2009).

In this case, to identify the number of research's that are thrown out, there are a few filters were excluded such as systematic review articles, review articles, meta-analysis articles, book series, book, book chapter, conference proceeding, English, published <2019, other than social science, non-Asian countries and etc which results in 265 research documents. (Liberati, 2009).

Out of the initial pool of 430 papers obtained from both Scopus and Web of Science, a total of 165 documents were filtered and selected for inclusion in this research. The selection process involved a rigorous screening approach aimed at establishing a conclusive study set that met specific criteria. The main objective of this screening process was to ensure that the chosen papers provided a comprehensive, unbiased, and up-to-date representation of the topic being investigated. By adhering to strict criteria for inclusion, the aim was to gather findings that were thorough, objective, and reflective of the current understanding of the subject matter being evaluated. (Liberati, 2009).

### 2.1.3 Eligibility Method

In the context of evaluating research literature, the eligibility approach involves establishing criteria for the inclusion and exclusion of studies. This systematic process is essential to ensure a comprehensive review that reflects the current knowledge on a specific topic. Researchers employ various factors, such as standards for assessing the quality of research design, appropriate sample sizes, recent publication dates, and authenticity assessments of evidence, to accurately select literature sources eligible for inclusion in their reviews. By employing this eligibility technique, biases are minimized, and exceptional literature sources with reliable information are chosen. This approach contributes to the overall validity and credibility of the study. (Moher et al., 2010).

During the course of this investigation, a comprehensive search yielded a total of 165 papers that were potentially relevant to the topic of Ahmed Body and Drag. Considering the large number of papers, a screening process was implemented to identify the most relevant articles and documents for the research question at hand. Keywords such as Skin friction, Computational Fluid Dynamics (CFD), fluid dynamics, dimple, Drag Reduction, Flow Control, dimple, and Drag Force were employed to refine and narrow down the publications in both Scopus and Web of Science databases. This keyword-based approach helped to link and restrict the selection of papers, ensuring a focused and targeted review. (Moher et al., 2010).

Additionally, a few papers couldn't be utilised without permission, thus an all-open access filter was used for convenience. Additionally, other documents dealt with unrelated topics including Earth and Planetary Sciences, Multidisciplinary, Decision Sciences, Social Sciences, and Chemistry. (Moher et al., 2010).



#### 2.1.4 Inclusion Method

Anyone undertaking a research literature analysis should employ careful methods during their selection process known as the "inclusion method." This meticulous technique involves both narrowly defining search parameters while also establishing rigorous standards when selecting articles from said searches – notably by considering factors such as study design or subject relevance to prevent any possible biases from creeping into their analysis work. Ultimately this approach produces reviews reflecting current knowledge levels achieved from available material – making them more comprehensive and useful for researchers or anyone else looking to understand a specific topic better. (Page & Moher, 2017).

After limiting the unwanted things out of the search webs, a few documents that are highly related to the topic or study in hand which is about 27 documents from both Scopus and Web of Science were taken to be included as quality synthesis. The techniques, results, and conclusions of the study, as well as supplemental data pertaining to the research issue, are all carefully examined in this review. (Liberati, 2009).

The data were gathered and synthesised to the research question using the inclusion technique, and the eligible studies that fit the inclusion conditions are included in the final analysis. By choosing studies that meet the pre-established eligibility criteria and rejecting those that did not, this strategy also makes sure that the final analysis is based on high-quality data that is pertinent to the research question. (Krappel et al., 2014).

## 2.2 Outcome of SLR

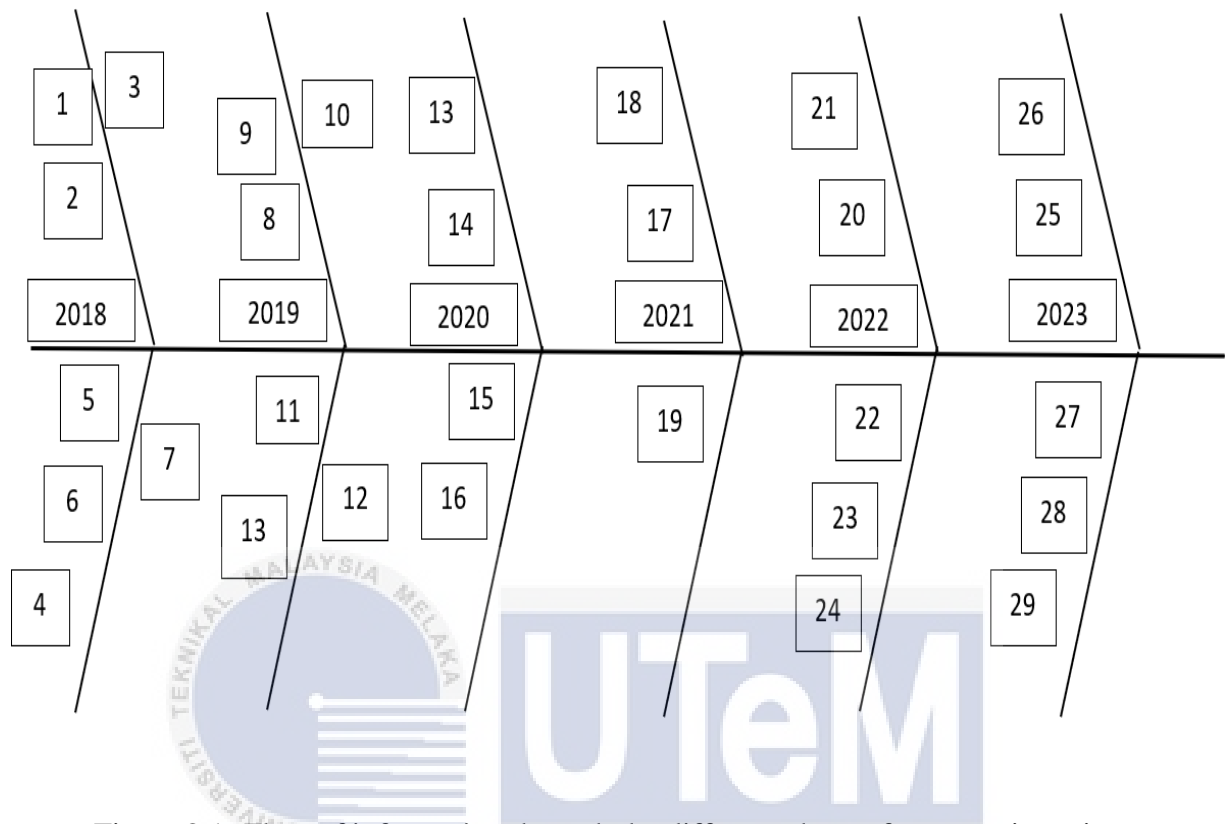


Figure 2.1 Flow of information through the different phase of systematic review

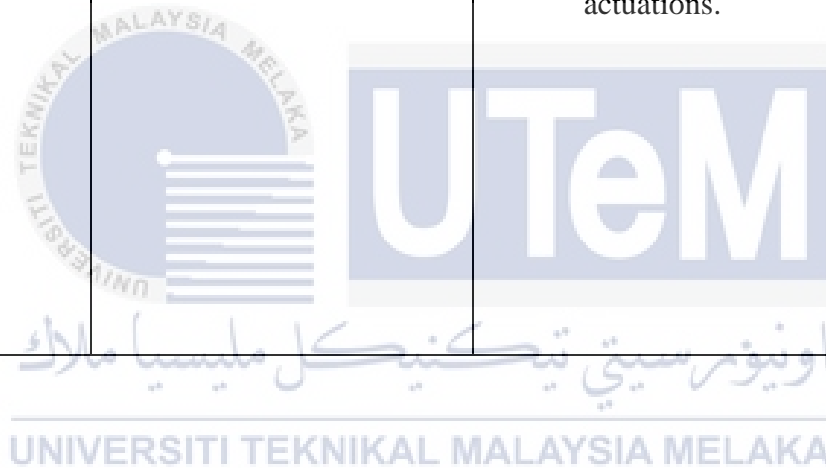
اونيورسيتي تيكنيكل مليسيا ملاك

UNIVERSITI TEKNIKAL MALAYSIA MELAKA

### 2.2.1 Table Author & Findings

Table 2.1 Author and findings according to year published

BIL	YEAR	AUTHOR	FINDINGS
1.	2018	Zhang, B.F., Liu, K., Zhou, Y., To, S., Tu, J.Y.	<ul style="list-style-type: none"><li>• Experimental investigation of active drag reduction on an Ahmed body with a slant angle. Reynolds number-based study achieves 6-14% drag reduction using separate steady blowing actuations.</li></ul>



2.	2018	<u>Sardana, H., Singh, M.</u>	<ul style="list-style-type: none"> <li>• Research aims to reduce SUV drag using a vortex generator, analysing pressure and turbulence profiles. CFD simulations compare performance with and without the generator at various velocities, seeking the velocity with the lowest drag.</li> </ul>
3.	2018	<u>Buscariolo, F.F., Sherwin, S.J., Assi, G.R.S., Meneghini, J.R.</u>	<ul style="list-style-type: none"> <li>• Correlation study between computational and physical models of an Ahmed Body with a squared back. Physical results from wind tunnel test (STRACHAN et al., 2007) [11] and CFD simulations using Nektar++ with Spectral Vanish Viscosity - iLES-SVV turbulence model.</li> </ul>
4.	2018	<u>Devanuri, J.K.</u>	<ul style="list-style-type: none"> <li>• Air brake use increases drag coefficient with height and angle of inclination.</li> <li>• Surprising results show drag coefficient varies with position: maximum at foremost point,</li> </ul>

			<p>decreases and then increases as air brake moves towards the rear.</p> <p>Increasing air brake height reduces drag coefficient when positioned towards the rear.</p>
5.	2018	<u>Edwige, S., Eulalie, Y., Gilotte, P., Mortazavi, I.</u>	<ul style="list-style-type: none"> <li>• Low-frequency modes dominate flow dynamics, with a notable pressure mode (Strouhal number 0.22) causing aerodynamic losses near the rear.</li> </ul>
6.	2018	<u>Filip, G., Maki, K., Bachant, P., Lietz, R.</u>	<ul style="list-style-type: none"> <li>• Evaluation of vortex generators for vehicle drag reduction using CFD and experimental validation.</li> </ul>
7.	2018	<u>Rao, A., Minelli, G., Basara, B., Krajnović, S.</u>	<ul style="list-style-type: none"> <li>• Flow states I and II compared for lift and drag coefficients in the 25° back slant Ahmed body.</li> <li>• Aspect ratio affects flow states: low aspect ratio corresponds to flow state II, while large aspect ratio corresponds to flow state I.</li> <li>• Yaw angle (<math>\beta</math>) influences flow states in the 35° back slant Ahmed body: <math> \beta  \lesssim 12.5^\circ</math> results in flow state I, and <math> \beta  = 15^\circ</math> results</li> </ul>



			in flow state II with stronger vortices aiding flow reattachment.
--	--	--	---



8.	2019	Igali, D., Mukhmetov, O., Zhao, Y., Fok, S.C., Teh, S.L.	<ul style="list-style-type: none"> <li>• RANS approach with skillful mesh and proper discretization captures complex flow over 25° Ahmed body as effectively as LES solvers, with SST model performing best.</li> </ul>
9.	2019	<u>Kumar, A., Singh, S., Bhalla, N.A.</u>	<ul style="list-style-type: none"> <li>• Numerical analysis of 2D Ahmed body models using CFD reveals drag coefficient and flow characteristics.</li> </ul>
10.	2019	<u>Wang, B., Yang, Z., Zhu, H.</u>	<ul style="list-style-type: none"> <li>• New actuators alter flow topology, pressure distribution, and flow process, reducing drag up to 25.5%.</li> </ul>
11.	2019	<u>Thomas, B., Agarwal, R.K.</u>	<ul style="list-style-type: none"> <li>• Computational results show that k-ε realizable, k-ω SST and WA models yield values closer to the experimental data with WA model requiring less simulation time per iteration than the other two models.</li> </ul>
12.	2019	<u>Buscariolo, F.F., Meneghini, J.R., da Silva Assi, G.R., Sherwin, S.J.</u>	<ul style="list-style-type: none"> <li>• High-fidelity CFD method with Spectral/hp element discretization used for better accuracy.</li> <li>• Diffuser length fixed at 222mm, angle varied from 0° to 50° in 10° increments.</li> </ul>

13.	2019	<u>Liu, K., Zhang, B.F., Zhou, Y.</u>	<ul style="list-style-type: none"> <li>• Steady blowing is used on upper and side edges of rear window and upper edge of vertical base.</li> <li>• Drag is reduced by 25%, surpassing literature-reported reductions for similar bodies.</li> <li>• Effective technique for maximizing drag reduction.</li> </ul>
14.	2020	Karimi, S., Zargar, A., Mani, M., Hemmati, A.	<ul style="list-style-type: none"> <li>• SDBD actuators improved Ahmed body's aerodynamic performance.</li> <li>• Different arrangements of actuators were tested for drag reduction.</li> <li>• The most effective arrangement resulted in approximately 6.1% drag reduction.</li> <li>• SDBD altered three-dimensional wake structures and surface pressure on the body, contributing to the improvement.</li> </ul>
15.	2020	<u>Fan, D., Zhang, B., Zhou, Y., Noack, B.R.</u>	<ul style="list-style-type: none"> <li>• Sacrificing a small amount of performance yields significant actuation power savings.</li> <li>• Findings offer valuable guidance for future drag reduction studies and engineering applications.</li> </ul>

16.	2020	<u>Mohammadikalakoo, B., Schito, P., Mani, M.</u>	<ul style="list-style-type: none"> <li>• Objective: Develop passive drag reduction devices for bluff body vehicles.</li> <li>• Purpose: Reduce vehicle fuel consumption by reducing drag.</li> <li>• Methods: Passive and active techniques are employed.</li> <li>• Reference Model: Ahmed Body with slant angles of 25°, 30°, and 35°.</li> <li>• High-pressure flow movement reduces wake size and pressure drag.</li> </ul>
17.	2020	<u>Mariette, K., Bideaux, É., Bribiesca-Argomedo, F., (...), Castelain, T., Michard, M.</u>	<ul style="list-style-type: none"> <li>• Study focuses on bluff bodies with wake asymmetries caused by natural biostability or crosswind.</li> <li>• Nonlinear controller tuned using pulsed jet actuators on modified Ahmed bluff body.</li> <li>• Wake symmetrisation achieved in aligned or crosswind configurations.</li> <li>• Aim: Reduce drag increase at high velocities.</li> </ul>
18.	2021	<u>Liu, K., Zhang, B., Zhou, Y.</u>	<ul style="list-style-type: none"> <li>• Drag/pressure variations with different blowing combinations can</li> </ul>

			<p>be represented by two local pressures on the rear window and base.</p> <ul style="list-style-type: none"> <li>• The correlation between drag and a linear combination of the two local pressures is approximately linear.</li> </ul>
19.	2021	<u>Koppa Shivanna, N., Ranjan, P., Clement, S.</u>	<ul style="list-style-type: none"> <li>• Modification of afterbody shape reduces drag by altering wake topology.</li> <li>• Inclusion of cavity and modifications decrease flow randomness, reducing chaotic nature in wake.</li> <li>• Cavity presence increases vorticity spreading rate in mixing layer.</li> </ul>
20.	2021	<u>Buscariolo, F.F., Assi, G.R.S., Sherwin, S.J.</u>	<ul style="list-style-type: none"> <li>• Ahmed body with 25° slant angle and a diffuser</li> <li>• Peak downforce at 20° diffuser angle due to two streamwise vortices and flow separation</li> <li>• Peak drag at 30° diffuser angle with full flow separation.</li> </ul>
21.	2022	<u>The Hung, T., Hijikuro, M., Anyoji, M., (...), Nakashima, T., Shimizu, K.</u>	<ul style="list-style-type: none"> <li>• Deflector reduces drag at low yaw angles.</li> <li>• Breakdown of longitudinal vortexes and separation bubble cause separated flow on slant leading edge.</li> </ul>

22.	2022	<u>Siddiqui, N.A., Agelin-Chaab, M.</u>	<ul style="list-style-type: none"> <li>Investigation results: Body modification of Ahmed body with elliptical curvature at rear end affects flow features.</li> <li>Conclusion: Significant improvement in vehicles' aerodynamic performance through this modification.</li> </ul>
23.	2022	<u>Tran, T.H., Anyoji, M., Nakashima, T., Shimizu, K., Le, A.D.,</u>	<ul style="list-style-type: none"> <li>Technique effectively extracts skin-friction topology</li> <li>Cross-wind has minimal impact on flow for yaw angle below 3 deg</li> <li>Drag of the model remains constant</li> </ul>
24.	2022	<u>Edwige, S., Gilotte, P., Mortazavi, I.</u>	<ul style="list-style-type: none"> <li>Shear layer variations seen during blowing phase</li> <li>Main flow topology change caused by suction and synthetic jets</li> <li>Rear back pressure significantly increased</li> </ul>
25.	2022	<u>Passaggia, P.-Y., Mazellier, N., Kourta, A.</u>	<ul style="list-style-type: none"> <li>Increasing free-stream turbulence causes a significant shift in wake meandering dynamics.</li> </ul>

			<ul style="list-style-type: none"> <li>• The wake transitions from intermittent to Gaussian behavior.</li> <li>• Higher free-stream turbulence results in decreased wake amplitude, frequency, and spatial distribution.</li> </ul>
26.	2023	Siddiqui, N.A., Agelin-Chaab, M.	<ul style="list-style-type: none"> <li>• EAB at 26° performed at <math>1.9 \times 10^5</math> achieves fully detached flow.</li> <li>• Flow is completely detached with no C-vortices or lower recirculation bubbles.</li> <li>• This structure reduces drag by approximately 21% and prevents soiling.</li> </ul>
27.	2023	<u>Darabasz, T., Bonnavion, G., Cadot, O., Goragner, Y., Borée, J.</u>	<ul style="list-style-type: none"> <li>• Drag reduction: 11.5%</li> <li>• Wake structure respects symmetry of body base in lateral and vertical directions.</li> <li>• Full stabilization of initial steady instability observed.</li> <li>• Longitudinal vortex pair forms at imprint edges, penetrating recirculating area.</li> </ul>

28.	2023	<u>Nayakar, K., Ramayana, Supradeepan, K., Gurugubelli, P.S.</u>	<ul style="list-style-type: none"> <li>• Simulations conducted using the K-omega SST turbulence model in ANSYS 2021 Academic.</li> <li>• Results obtained from the simulations.</li> </ul>
29.	2023	<u>Deng, G.M., Fan, D.W., Zhang, B.F., Liu, K., Zhou, Y.</u>	<ul style="list-style-type: none"> <li>• Efficiency exceeds Fan et al.'s (2020) result of 26.5.</li> <li>• Fan et al. used only three independent control parameters.</li> </ul>





## 2.3 Design

### 1. YEAR OF 2018

Experimental Investigation of Flow Control over an Ahmed Body using DBD Plasma Actuator

Ahmed body is a standard configuration of road vehicles and most of the studies of automobile aerodynamics are performed based on it. In this paper, the plasma actuator was used as an active flow control method to control the flow around the rear part of the Ahmed body with the rear slant angle of  $25^\circ$ . Experiments were carried out in a wind tunnel at two different velocities of  $U=10\text{m/s}$  and  $U=20\text{m/s}$  using steady and unsteady excitations. The hot-wire anemometer was used to measure the vortex shedding frequency at the downstream of the body. Pressure distribution was measured using 52 sensors and total drag force was extracted with a load cell. (S. Shadmani<sup>1</sup>, S. M. Mousavi Nainiyan<sup>1†</sup>, M. Mirzaei<sup>2</sup>, R. Ghasemiasl<sup>1</sup> and S. G. Pouryoussefi<sup>2</sup>)

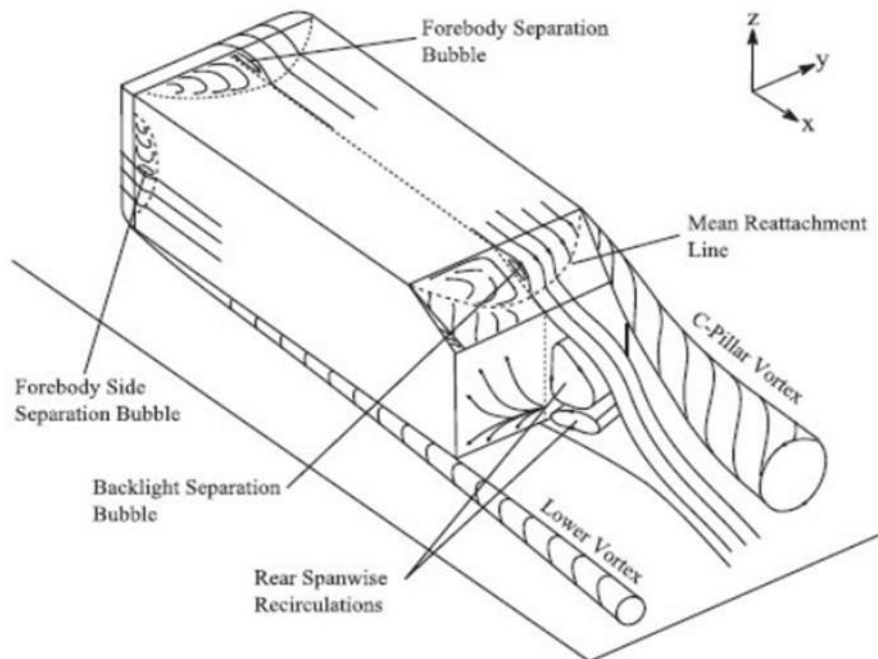


Figure 2.2 Experimental Investigation of Flow Control over an Ahmed Body using DBD Plasma Actuator,



## 1. Aerodynamic drag reduction and flow control of Ahmed body with flaps

In this study, the researcher attempted a novel drag reduction technique for 25 and 35 Ahmed models by experimenting with two types of flap structures, respectively, added to the slant edges of the two models. Different pairs of flaps were added at various angles compared to the slant for the sake of comparison. The study comprehensively analysed the effects of the “big-type” and “small-type” flaps on the aerodynamic drag and near wake of an Ahmed model in a greater range of flap mounting angles. Parametric analysis results confirmed that large and small flaps are most efficient when configured on the 25 Ahmed model at specific angles; up to 21% pressure coefficient reduction was achieved for the 25 Ahmed model (flap configurations at slant side edge) and 6% for the 35 Ahmed model (flap configurations at both slant side and top edges). The velocity and pressure contours indicated that the key to drag reduction is to weaken (if not eliminate) the longitudinal vortex created at the side edges of the rear slant. (Jie Tian, Yingchao Zhang, Hui Zhu and Hongwei Xiao)

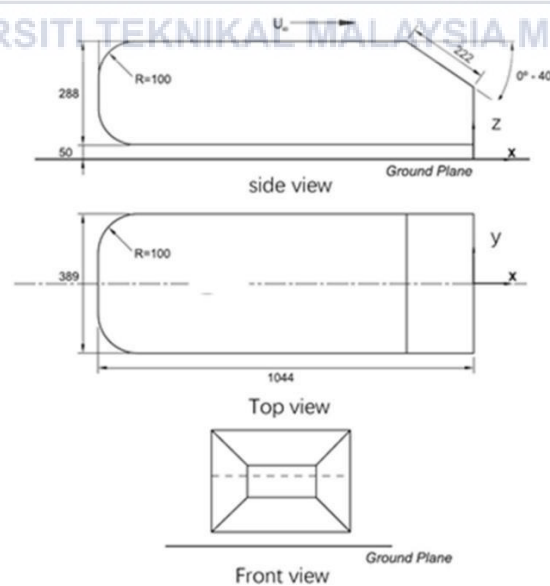


Figure 2.3 Ahmed body dimensions

## 2. YEAR OF 2019

### 1. Effect of slant angle variation on the drag force for Ahmed body car model

In this paper, numerical investigation is carried out on two-dimensional Ahmed body model using Computational Fluid Dynamics in ANSYS Fluent 19.1. The 2-D model is designed in Catia v5 for 25°, 35° and 45° slant angles. The turbulent model used to analyse the flow dynamics is Realizable k- $\epsilon$  model. The dragcoefficient variation with respect to slant angle is computed. The skin friction coefficient, wall shear stress and frictional velocity are also calculated. (Ashish Kumar, Srijna Singh, Neelanchali Asija Bhalla)

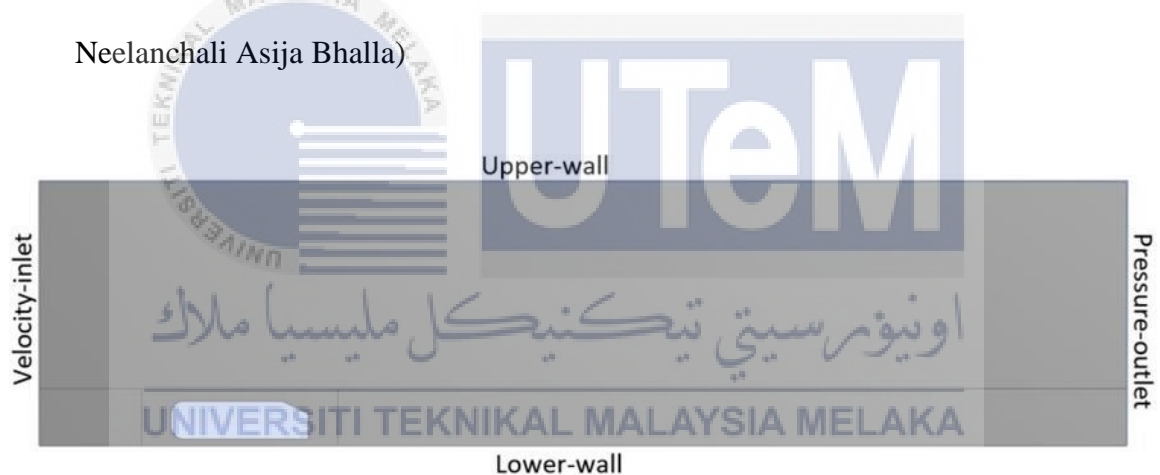
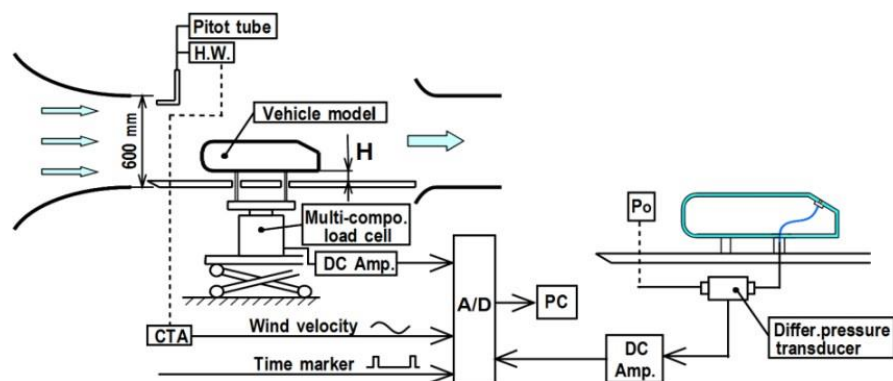


Figure 2.4 : Ansys view of Ahmed model

## 2. Aerodynamic Forces Acting on Ahmed-Type Vehicles under Fluctuating Headwind Conditions

Aerodynamic forces of Ahmed-type Road vehicles subjected to atmospheric fluctuation were studied in an advanced wind tunnel with programmable settings enabling the generation of pulsating wind speeds. The experiments were performed with a time-averaged airflow speed of approximately 13 m/s, with the fluctuating speed ranging from 2.58 to 2.90 m/s, and periods ranging from 1.5 to 5.0 s. The results of the time-dependent drag and lift forces acting on the vehicle were compared with those under steady wind conditions. Further, the influence of the rear slant angle of the Ahmed model on the forces was addressed. The fluctuation in wind speed showed a greater effect on the aerodynamic forces than predicted. The amplitude of the drag force under the pulsating wind became larger in a vehicle having a shape that experienced a large drag force under steady wind conditions. It is concluded that even under fluctuating wind conditions, there exists a critical angle of  $30^\circ$  which the vehicle experiences either high or low fluid forces. (M. Sumida and K. Hayakawa)

Figure 2.5 : Fluctuating Headwind Conditions



## YEAR OF 2020

1. This paper reports a numerical investigation of the effect of aspect ratio (AR) on the flow structure around the  $35^\circ$  Ahmed body. The AR is defined as the ratio of length to the height of the model. A total of five ARs are considered at a Reynolds number based on the height of the Ahmed body of  $7.8 \times 10^5$ . The flow governing equations are solved in the FLUENT solver using the SST K-Omega turbulence model. It is found that the drag coefficient ( $C_d$ ) slightly increases at the AR1 4.2%. As the aspect ratio increases, the drag coefficient decreases. The analysis reveals that early flow separation in the AR1 causes a reattachment at the rear slant end, which leads to an increase in drag. It also highlights that there exists a minimum aspect ratio beyond which the drag increases, and there is a limit in the increasing order beyond which the drag will begin to reduce. Further, it demonstrates that there is no change in the recirculation region and consequently drag coefficient is not a function of the recirculation region. Thence, a clear understanding of the effect of the length-based aspect ratio can help to optimize the length during design. (Naseeb Ahmed Siddiqui & Martin Agelin-Chaab)

## 2. The Effect of Single Dielectric Barrier Discharge Actuators in Reducing Drag on an Ahmed Body

The feasibility of a single dielectric barrier discharge (SDBD) actuator in controlling flow over an Ahmed body, representing a simplified car model, has been numerically and experimentally investigated at Reynolds numbers of  $7.68 \times 10^5$  and  $2.25 \times 10^5$ . The Ahmed body had slant angles of  $25^\circ$  and  $35^\circ$ . The results showed that SDBD actuators could significantly enhance the aerodynamic performance of the Ahmed body. Several arrangements of the actuators on the slant surface and the rear face of the model were examined to identify the most effective arrangement for drag reduction. This arrangement resulted in an approximately 6.1% drag reduction. This improvement in aerodynamic performance is attributed to the alteration of three-dimensional wake structures due to the presence of SDBD, which coincides with surface pressure variations on the slant and rear faces of the Ahmed body. (Saber Karimi, Arash Zargar, Mahmoud Mani and Arman Hemmati 2)

UNIVERSITI TEKNIKAL MALAYSIA MELAKA

### 3. A Simple Passive Device for the Drag Reduction of an Ahmed Body

In this paper, a simple passive device is proposed for drag reduction on the 35° Ahmed body. The device is a simple rectangular flap installed at the slant surface of the model to investigate the effect of slant volume, formed between the device and the slant surface, on the flow behaviour. The slant volume can be varied by changing the flap angle. This investigation is performed using the FLUENT software at a Reynolds number of  $7.8 \times 10^5$  based on the height of the model. The SST k-omega model is used to solve the Navier-stokes equations. It is found that this passive device influences the separation bubbles created inside the slant volume and provides a maximum drag reduction of approximately 14% at the flap angle of 10°. Moreover, the device delays the main separation point, which changes the flow conditions at the back of the model. The drag reduction was found to mainly dependent on the suppression of the separation bubbles formed inside the slant volume, which leads to faster pressure recovery. The cause of this pressure recovery is found to be the reduction in recirculation length and width. (N. A. Siddiquim and M. A. Chaab)



#### 4. A CFD Tutorial in Julia: Introduction to Compressible Laminar Boundary-Layer Flows

A boundary-layer is a thin fluid layer near a solid surface, and viscous effects dominate it. The laminar boundary-layer calculations appear in many aerodynamics problems, including skin friction drag, flow separation, and aerodynamic heating. A student must understand the flow physics and the numerical implementation to conduct successful simulations in advanced undergraduate and graduate-level fluid dynamics/aerodynamics courses. Numerical simulations require writing computer codes. Therefore, choosing a fast and user-friendly programming language is essential to reduce code development and simulation times. Julia is a new programming language that combines performance and productivity. (Furkan Oz and Kursat Kara)

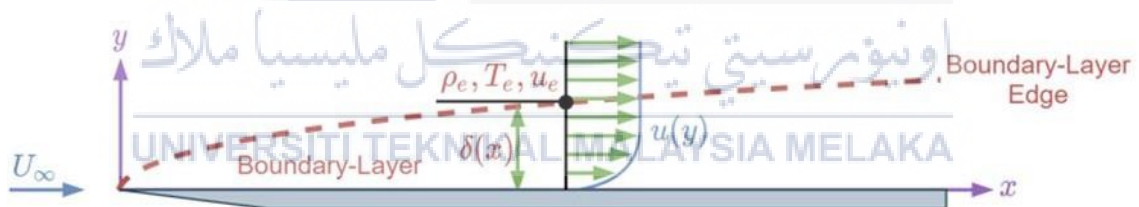


Figure 2.6 : Compressible Laminar Boundary-Layer Flows

## YEAR OF 2021

### 1. Computational study on an Ahmed Body equipped with simplified underbody diffuser

The Ahmed body is one of the most studied 3D automotive bluff bodies and the variation of its slant angle of the rear upper surface generates different flow behaviours, similar to a standard road vehicle. In this study we extend the geometrical variation to evaluate the influence of a rear underbody diffuser which are commonly applied in high performance and race cars to improve downforce. Parametric studies are performed on the rear diffuser angle of two baseline configurations of the Ahmed body: the first with a 0 upper slant angle and the second with a 25-slant angle. We employ a high-fidelity CFD simulation based on the spectral/hp element discretisation that combines classical mesh refinement with polynomial expansions in order to achieve both geometrical refinement and better accuracy. The diffuser length was fixed to the same length of 222 mm similar to the top slant angle that have previously been studied. The diffuser angle was changed from 0 to 50 in increments of 10 with an additional case considering the angle of 5. The proposed methodology was validated on the classical Ahmed body considering 25 slant angles, found a difference for drag and lift coefficients of 13% and 1%, respectively. For the case of a 0-slant angle on the upper surface the peak values for drag and negative lift (downforce) coefficient were achieved with a 30-diffuser angle, where the flow is fully attached with two streamwise vortical structures, analogous to results obtained from [1] but with the body flipped upside down. For diffuser angles above 30, flow is fully separated from the diffuser. (Publisher: Filipe F. Buscariolo, Gustavo R.S. Assi, Spencer J. Sherwin)

## YEAR OF 2022

### 1. Explorative gradient method for active drag reduction of the fluidic pinball and slanted Ahmed body

We address a challenge of active flow control: the optimization of many actuation parameters guaranteeing fast convergence and avoiding suboptimal local minima. This challenge is addressed by a new optimizer, called the explorative gradient method (EGM). EGM alternatively performs one exploitive downhill simplex step and an explorative Latin hypercube sampling iteration. Thus, the convergence rate of a gradient based method is guaranteed while, at the same time, better minima are explored. For an analytical multi-modal test function, EGM is shown to significantly outperform the downhill simplex method, the random restart simplex, Latin hypercube sampling, Monte Carlo sampling and the genetic algorithm. ( Yiqing Li, Wenshi Cui, Qing Jia, Qiliang Li, Zhigang Yang, Marek Morzynski and Bernd R. Noack)

## 2. Wake transitions and steady z-instability of an Ahmed body in varying flow conditions

The paper investigates experimentally the flow past a flat-back, taller than wide Ahmed body having rectangular base aspect ratio  $H/W = 1.11$  in the context of ground vehicle aerodynamics. Parametric studies at Reynolds number  $2.1 \times 10^5$  explore the sensitivity of the aerodynamic force and body pressure distribution with respect to varying flow conditions defined from variable ground clearance  $C$  (taken at mid-distance from the front and rear axles of the body), pitch angle  $\alpha$ , and yaw angle  $\beta$  (equivalent to a crosswind). Two-dimensional parametric maps in the parametric spaces  $(\beta, C)$  and  $(\beta, \alpha)$  are obtained for parameter ranges covering real road vehicle driving conditions. (Yajun Fan, Vladimir Parezanovi and Olivier Cadot)

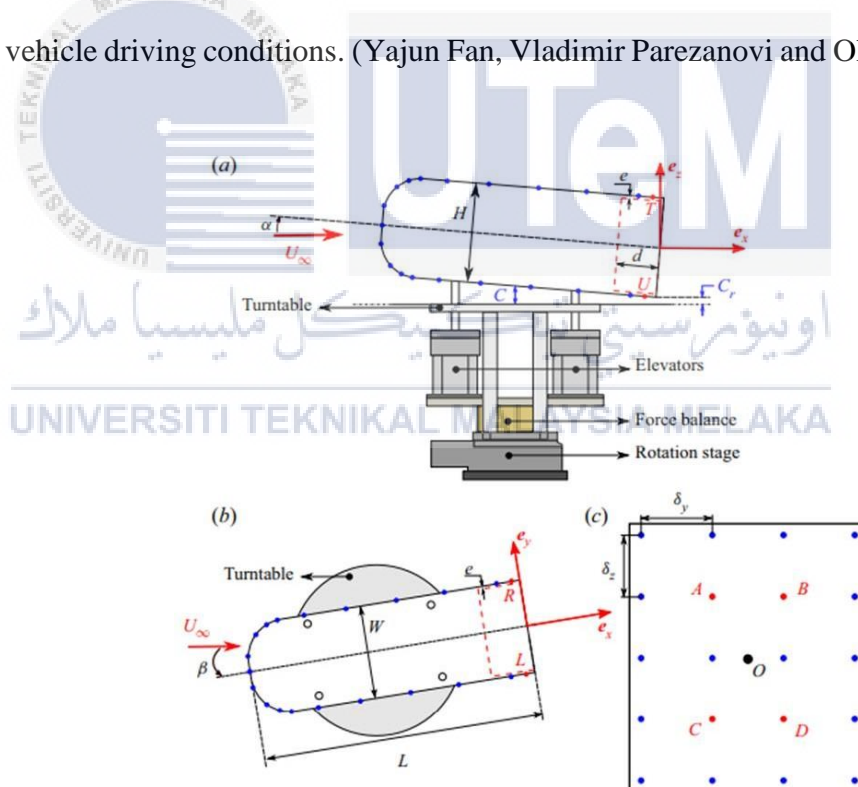


Figure 2.7 : Ahmed body in varying flow conditions

### 3. Investigation of the Aerodynamic Characteristics of Platoon Vehicles Based on Ahmed Body

In this paper, the aerodynamic characteristics of two vehicles and three vehicles in the platoon under different vehicle spacings have been explored in detail. Firstly, the realizable k- $\epsilon$  model was used to verify the numerical method based on a single 35° Ahmed body. The aerodynamic characteristics such as drag characteristics, surface pressure, wake structure, and turbulent kinetic energy distribution were analysed for the platoon of two and three 35° Ahmed bodies. Although the RANS (Reynolds-averaged Navier–Stokes) model had got good results for simulating a single 35° Ahmed body, when simulating two 35° Ahmed bodies in the platoon, it was found that there is still a big error compared with the experimental data. In the three 35° Ahmed body, the drag coefficient of the leading body is almost unchanged compared with that of the leading body in the two-vehicle platoon, while the drag coefficients of the middle body and the trailing body are both reduced compared with those of the single body. ( Jianbin Luo, Ke Mi, Dongli Tan, Zhiqing Zhang, Mingsen Li, Jun Qing and Huiqiong Huang)

#### 4. Passive Flow Control of Ahmed Body using Control Rod

In the current study, numerical analysis of passive control flow with a control rod for Ahmed body is performed at different slant angles and velocities and placed rod locations on the slant surface. The aim of the study is to improve aerodynamic performance by preventing flow separation on the slant surface of Ahmed body using a control rod. This passive flow control method uses a control rod that has not been applied for simplified ground vehicles before. Therefore, it can be said that this study is a new example in point of a passive flow control application for Ahmed body. The solution of the study is performed by using the Computational Fluid Dynamics (CFD) method. (A.Şumnu)



## YEAR OF 2023

### 1. Drag reduction using longitudinal vortices on a fat back Ahmed body

The paper presents different cavity wall designs at the rear of a fat-back Ahmed body to achieve drag reduction. The wake balance is assessed using the variance of the base pressure gradient and correlated to the obtained drag reduction. Without the rear cavity, the fat-back Ahmed body is subject to a steady instability producing a strong wake imbalance in the horizontal direction. The low drag rear design consists of a 5° inclined spoiler at the bottom (referred to as a diffuser) that first provokes a vertical imbalance and a non-inclined top spoiler with central imprints that re-balance the wake. The drag reduction is 11.5%, the wake structure is observed to respect the symmetry of the body base in both lateral and vertical directions suggesting a full stabilization of the initial steady instability. Both the wake balance and the stabilization are associated with the formation of a longitudinal vortex pair initiated at the imprint edges and penetrating the recirculating area. ( T. Darabasz, G. Bonnavion, O. Cadot<sup>3</sup>, Y. Goraguer and J. Borée)

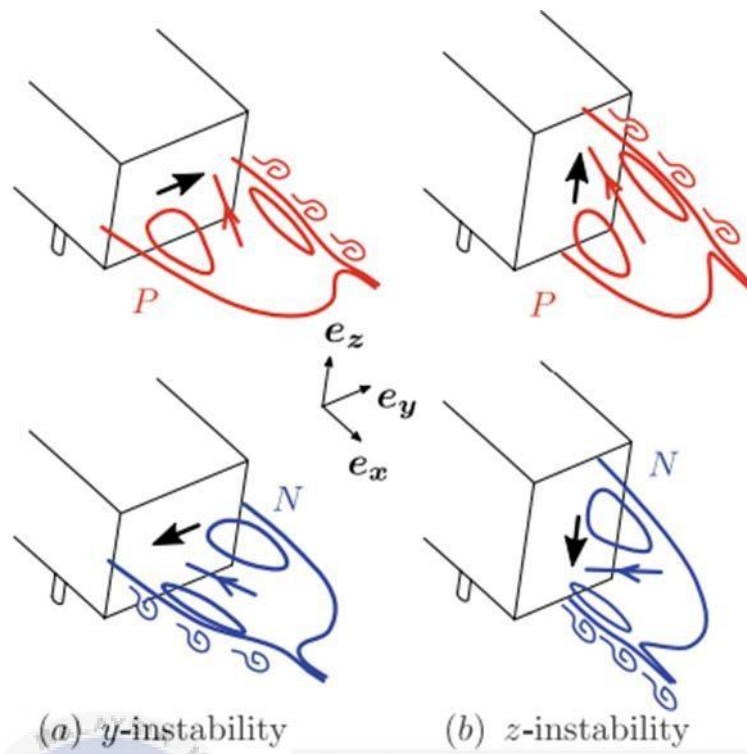
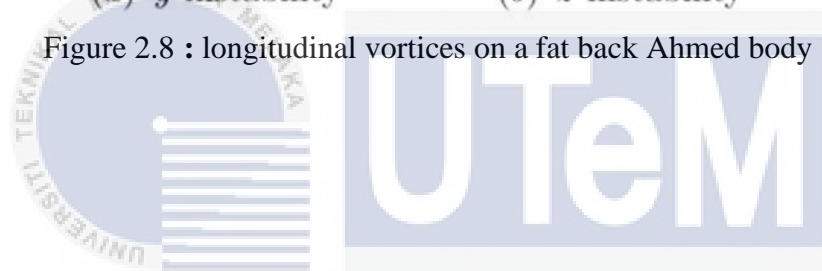


Figure 2.8 : longitudinal vortices on a fat back Ahmed body



اونيورسيتي تيكنيكل مليسيا ملاك

UNIVERSITI TEKNIKAL MALAYSIA MELAKA



## 2.4 Modelling

In the field of computational fluid dynamics (CFD), modelling plays a crucial role by employing mathematical equations to approximate and represent the real-world phenomena observed in fluid flows. This enables us, as university students, to gain a deeper understanding of fluid dynamics without the need for complex and computationally expensive calculations. Various modelling approaches are utilized to simplify and manage the simulations, as solving the complete set of governing equations for fluid flow can often be challenging and resource-intensive.

### 2.4.1 Meshing

In the realm of CFD simulations, meshing holds significance as it involves breaking down the computational domain into smaller finite elements or cells to represent the physical geometry accurately. By discretizing the domain through meshing, we can solve the governing equations for fluid flow and heat transfer using numerical methods. As university students, we understand the pivotal role of meshing in achieving accurate and efficient simulation results. The quality and resolution of the mesh directly impact the fidelity of our findings, making it a crucial aspect of CFD simulations.

Table 2.2 Comparison between the experiment data and simulated 35 Ahmed model.

Case	$C_p^*$	$C_k^*$	$C_s^*$	$C_b^*$
Experiment	0.2013	0.0138	0.0983	0.0892
CFD	0.1985	0.0118	0.0979	0.0890

Table 2.1 shows a comparison between the experimental data data1 and results based on the converged simulation of the 35 Ahmed model. Errors between the CFD results and wind tunnel experiment results were small, so the errors meet the engineering application requirement of 5%.

Table 2.3 Comparison of standard 25 Ahmed model with Top\_big\_20 and Top\_small\_40.

Case	$C_p^*$	$C_k^*$	$C_s^*$	$C_b^*$
Standard	0.2463	0.0055	0.1427	0.0981
Top_big_20	0.2021	0.0093	0.0813	0.1115
Top_small_40	0.2025	0.0085	0.0956	0.0984



## 2.4.2 Turbulence model

In the realm of computational fluid dynamics (CFD), we rely on turbulence models to simulate and capture the intricate nature of turbulence in fluid flow. Turbulence, characterized by its chaotic and irregular fluid motion at high Reynolds numbers, gives rise to fluctuations in essential flow properties such as velocity, pressure, and more. As university students delving into the intricacies of CFD, we recognize the paramount importance of employing turbulence models to accurately portray and understand the dynamic behavior of fluid flows affected by turbulence.

Turbulence models, within the realm of fluid dynamics, encompass mathematical equations or closures that aim to approximate the complex behavior of turbulence, relying on a range of assumptions and simplifications. These models serve a crucial purpose in predicting the characteristics of turbulent flow within a specific fluid domain, accounting for phenomena like turbulent eddies, energy dissipation, and the interplay between various scales of turbulence. As university students exploring the fascinating field of fluid dynamics, we comprehend the significance of employing turbulence models to gain insights into turbulent flows. It's worth noting that there exist diverse types of turbulence models, each characterized by its unique set of assumptions and level of intricacy.

Reynolds-Averaged Navier-Stokes (RANS) Models, as extensively cited by Ghai et al. (2022) and Zhang et al. (2008), stand as the predominant turbulence models employed in various studies. These models assume that flow properties can be decomposed into a time-averaged mean component and a fluctuating turbulent component. Within the realm of RANS models, noteworthy examples include the k-epsilon model, the k-omega model, and the Reynolds Stress Model (RSM). For

instance, in a study focused on flow structure and heat transfer on the endwall surface, the  $k-\omega$  (SST) turbulence model was selected among other turbulent models due to its superior performance at low Reynolds numbers. This particular model allowed for a more accurate prediction of the Nusselt number and friction factor (Du et al., 2019). Similarly, when investigating turbulent flow characteristics through a  $90^\circ$  pipe bend, the RANS equations were employed, utilizing the  $k-\omega$  (SST) turbulence model as highlighted by Nandi (2021). A similar study examining pipe bends with guide vanes was conducted by Reghunathan Valsala et al. (2019).

Direct Numerical Simulation (DNS) emerges as a remarkably precise approach that directly tackles the Navier-Stokes equations without resorting to turbulence modeling. By bypassing the need for models, DNS offers a comprehensive and precise portrayal of turbulent flow phenomena. However, it is worth noting that DNS comes with computational expenses and is typically limited to relatively low Reynolds number flows, as Ghai et al. (2022) have highlighted. In this study, the simulations were conducted using a body-fitted grid comprising  $1280 \times 148 \times 152$  points in the x-, y-, and z-directions. The mesh employed is non-uniform across all three directions, with particular refinement near solid surfaces to ensure accuracy and capture intricate flow features.

### 2.4.3 Grid

In the realm of computational fluid dynamics (CFD) simulations, grid modelling—also referred to as grid generation or meshing—entails the creation of a discretized representation of the computational domain. This involves dividing the domain into smaller elements, such as cells or elements, to construct a structured grid or mesh structure. This grid serves as the foundation for solving the governing equations governing fluid flow and other relevant physical phenomena.

The significance of grid modelling in CFD simulations cannot be overstated, as it directly impacts the accuracy, efficiency, and reliability of the numerical solution. It becomes essential to construct a grid that adeptly captures the geometric intricacies and flow characteristics within the domain. Furthermore, the grid must fulfil certain criteria, such as quality and resolution, to ensure the stability and precision of the simulations. As university students exploring the nuances of CFD, we recognize the pivotal role of grid modelling in attaining accurate and reliable results.

In the research conducted by M. Moosa et al. (Moosa & Hekmat, 2019), it was found that the utilization of hybrid grid methods, which combine structured and unstructured grids, offers significant advantages in terms of reducing the number of grids and computational costs. For simulating incompressible steady fluid flow and heat transfer, a quadrilateral-type structured grid with a total of  $245 \times 95$  nodes (in X and Y directions, respectively) was employed. This grid configuration resulted in a deviation of approximately 0.330% and 0.372% for the Nu (Nusselt number) and f (friction factor), respectively, when compared to a larger grid size of  $370 \times 145$ . Consequently, for the remainder of the study, the grid with dimensions  $245 \times 95$  was chosen (Menni et al., 2019).

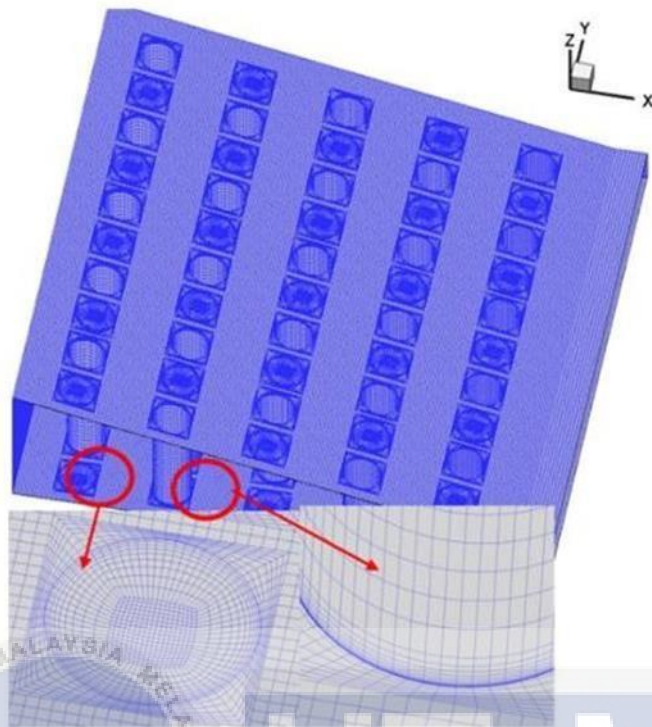


Figure 2.9 : Mesh Details (Du et al., 2019)

In the study conducted by Du et al. (2019), an internal code developed on the MATLAB platform was utilized to generate a multi-block structured grid. Upon increasing the mesh count from 4.0 million to 5.0 million, it was observed that both the Nusselt number and friction factor exhibited minimal changes. Consequently, a mesh count of 4.0 million was deemed suitable for all subsequent calculations. For further insight, Figure 2.1 provides detailed information regarding the mesh configuration.

## 2.5 Skin Friction

### 2.5.1 Introduction

Skin friction drag is a drag force caused by air molecules or fluid opposing the motion of an object (SKYbrary Wiki, 2021,13). Drag and lift forces behave differently on vehicles, aeroplanes, and trains because these applications need items to move in the opposite direction of the fluid flow. The friction of the fluid flow opposing the item moving towards it causes skin friction drag. As the air or fluid particles come into contact with a rough surface, the boundary layer and skin friction drag are directly proportional; greater area equals more drag. This phenomenon is not concerned with laminar flow fluid flow; but, at high velocities, it may impair the object's life cycle. Drag from turbulent flow has a negative impact on structural stability; thus, design considerations such as relative roughness, regulating smoothness, riveting, implementing smooth curves at joints, flat plates, adding painting and polishing layers, and so on are used to counteract.

One notable exploration study in this area is the disquisition of skin disunion reduction on the Ahmed body, which is a simplified model generally used in automotive aerodynamics. multitudinous studies have been conducted to assay different styles for reducing skin disunion on the Ahmed body, ranging from unresistant ways similar as face variations to active ways like the use of micro-textured shells or active inflow control.

There have been numerous previous studies on the Ahmed body, which is a simplified car model of 3D bluff shape; its front is designed to be blunt so that the flow cannot separate and aerodynamic forces depend instead largely on the flow structure created on the rear. The wake of the Ahmed model is a series of fully 3D complex flows which are directly linked to the coherent structures in the vehicle as reported by Vio and Watkins<sup>3</sup> and Beaudoin and Aider.<sup>4</sup> The flow structures contain three major components: The recirculation bubble over the rear slant, the longitudinal vortices created on the side edges or C-pillars of the slant, and the recirculation torus on the base of the model.





## 2.6 Terminology of Skin Friction

Skin friction drag is important for the body to be stable as well if the design considerations are not taken, it could increase energy consumption. Optimizing and minimizing friction drag can provide better stability, more control which impacts safety, and economic viability of using aircrafts, cars, and railways. Moreover, less friction drag helps these objects to move faster with higher velocities were optimizing and controlling drag will be crucial. The terminology related to skin friction commonly used in the field of fluid dynamics and aerodynamics includes Skin Friction Drag, Shear Stress, Boundary Layer, Boundary Layer Thickness, Friction Coefficient and Reynolds Number.

As an object moves through a fluid medium, it experiences various forms of resistance, including skin friction drag. This component constitutes an essential part of overall drag and arises from interactions between fluid molecules and surface bodies resulting in resistance arising from frictional forces. For instance, when fluids move over solid surfaces or boundaries as in aircraft wings or ship hulls, they experience shearing forces due to velocity gradients influencing molecule interactions at interfaces. Skin friction effects occur where such interactions lead to molecule sticking forces producing tangential forces on body surfaces- referred to as shear stress- resulting in parallel-generated drags called skin-friction drags.

The dimensionless friction coefficient links the frictional force acting on a body to the fluid dynamic pressure. When dealing with skin friction, it denotes the ratio between skin friction drag and fluid's dynamic pressure. This parameter is vital in estimating the level of skin grip encountered by a body travelling through a liquid medium. It offers uniform criteria for drawing comparisons between diverse flow conditions and geometries.

Mathematically, the friction coefficient ( $C_f$ ) is expressed as:

$$C_f = (\text{Skin Friction Drag}) / (\text{Dynamic Pressure})$$

where the skin friction drag is the component of drag force arising from skin friction, and the dynamic pressure is a measure of the kinetic energy per unit volume of the flowing fluid.



## 2.7 CFD and Altair

Understanding fluid mechanics phenomena requires specialized knowledge from computational fluid dynamics (CFD) experts who analyse and solve related issues using algorithms and numerical methods. Broadly used in prestigious sectors such as automotive, aerospace, energy production among others; CFD has enabled engineering fields to progress tremendously. Specifically speaking postulating Navier-Stokes equations has provided better insights towards capturing the conservation of mass, momentum, and energy factors in fluids that were deemed previously ambiguous. Moving forward, turbulence motion equations or species movements can be duly added when they are necessary.

Through its multifaceted offerings in Engineering Simulation and Data Analytics Software Solutions, Altair empowers engineers and managers across industries worldwide. The software ensures optimal product design and enhanced process productivity by providing an extensive variety of software solutions. These exceptional solutions consist of varied platforms that ingeniously integrate cutting-edge technology for sophisticated simulations presenting plausible evaluations. Altair's famed HyperWorks demonstrates its capability with tools such as Finite Element Analysis (FEA), Computational Fluid Dynamics (CFD) Electromagnetic Analysis alongside Multi-Body Dynamics analyses. These features make possible effective simulations while analysing structures as well as fluid movements within other physical systems.

## 2.8 Reynolds Number

To understand how fluids behave within a given system--a critical consideration for many industrial applications--engineers frequently turn to parameters such as the Reynolds number. This dimensionless value serves as an indicator of a fluids' flow regime by weighing factors such as skin friction against other variables like inertia and viscosity. By calculating this ratio scientists can distinguish between laminar versus turbulent flows and gain valuable insights into how different types of fluids will move throughout their respective systems. Mathematically speaking this key metric takes on the form of Re:

$$Re = (\text{Fluid Density} \times \text{Flow Velocity} \times \text{Characteristic Length}) / \text{Dynamic Viscosity}$$

Viscosity

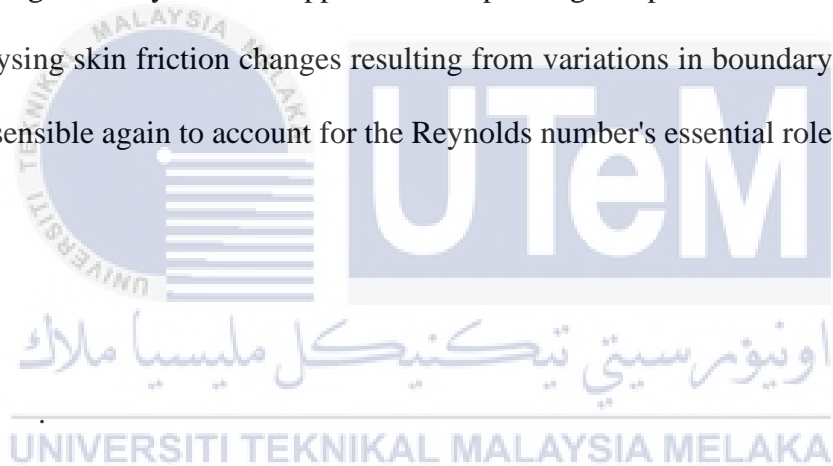
where:

- Fluid Density is the density of the flowing fluid.
- Flow Velocity is the velocity of the fluid relative to the body or within a conduit.
- Characteristic Length is a characteristic dimension of the flow geometry (e.g., body length, pipe diameter).
- Dynamic viscosity represents the measure of a fluid's resistance to flow, and it is a property of the fluid.

The behaviour of fluid flows hinges on whether they fall under the category of laminar or turbulent processes - an understanding that rests heavily on determining the Reynolds number. This important factor predicts how a given flow will behave: at low values of this parameter, we expect to observe smooth movement across

ordered layers of fluid with minimal mixing that characterizes pure laminar flows; at higher values, however, the situation rapidly transitions into one marked by unpredictable motion featuring high degrees of turbulence. In such cases where eddies and vortices define fluid behaviour often referred as turbulence, we witness an active exchange of energy and momentum resulting from enhanced mixing properties in fluids that exhibit it.

As each system has unique geometric configurations and environmental attributes that influence their dynamics at different ranges of Reynolds numbers, it precisely determines points where we observe shifts toward turbulence which can vary significantly between applications depending on specific circumstances. While analysing skin friction changes resulting from variations in boundary layer physics, it's sensible again to account for the Reynolds number's essential role.



## 2.9 Fuel Consumption

Considerable attention is currently being allocated towards Malaysia's surge in gasoline prices that have become an infamous topic across the nation. Among those severed by the rationalization made on gas subsidies are middle-class households who bear its dire consequences exceedingly. An interesting observation made is that vehicular aerodynamics play a vital role in determining excess gasoline usage with expanded frontal areas resulting in escalated drag force consequently increasing petrol consumption practices amongst drivers. For city buses servicing expenditure predominantly lies in its gasoline bills amounting to around 45% when traveling distances spanning around 80000km annually with fixed asset costs accounting for roughly around 40% (Nylund et al. 2007).

Volvo bus has provided useful information regarding its fleet's fuelling patterns over time for those equipped with DH12 engines. According to Edward Jobson's report (2013), vehicles utilizing this engine consume an estimated twenty-six litres worth of gas for every hundred kilometres driven at sixty kilometres per hour speeds on average. Meanwhile, Zhang et al.'s research project in prior studies applied a carbon balance technique to determine instantaneous fuel usage figures based real-time emissions levels from key carbon-based pollutants emitted from diesel-driven vehicles like common passenger buses which are typically expected to consume about thirty-two and six-tenths litres' worth for every hundred kilometres covered.

In a bid to reduce drag, significant attention was paid towards reshaping vehicle designs. Designers held sway over incorporating aerodynamic features into their car designs post-World War I [1]. Nevertheless, this endeavour could not yield

desired outcomes given design limitations and unavoidable space issues that arose from a vehicle's primary purpose being human transportation [2]. A streamlined body was unsuitable for boxy and bulky vehicles in the bluff body segment. Moreover, there was prevalent scarcity of sufficient storage space among these vehicles; hence adding an extra storage compartment fitted atop many MPVs.



## CHAPTER 3

### METHODOLOGY

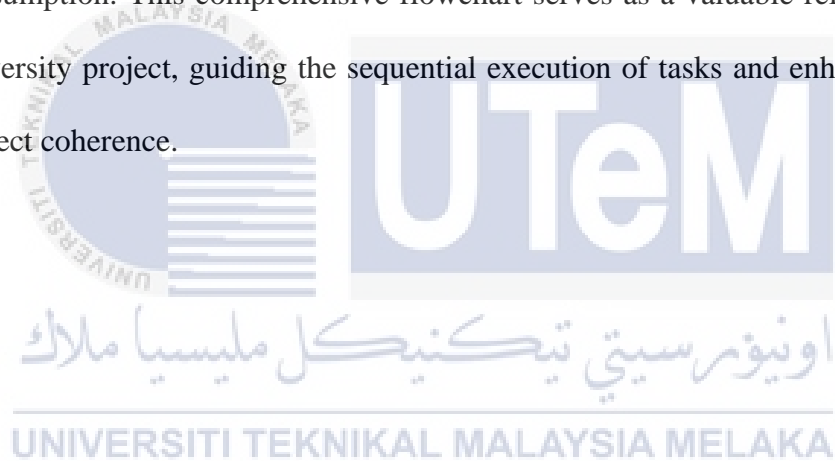
#### 3.1 Introduction

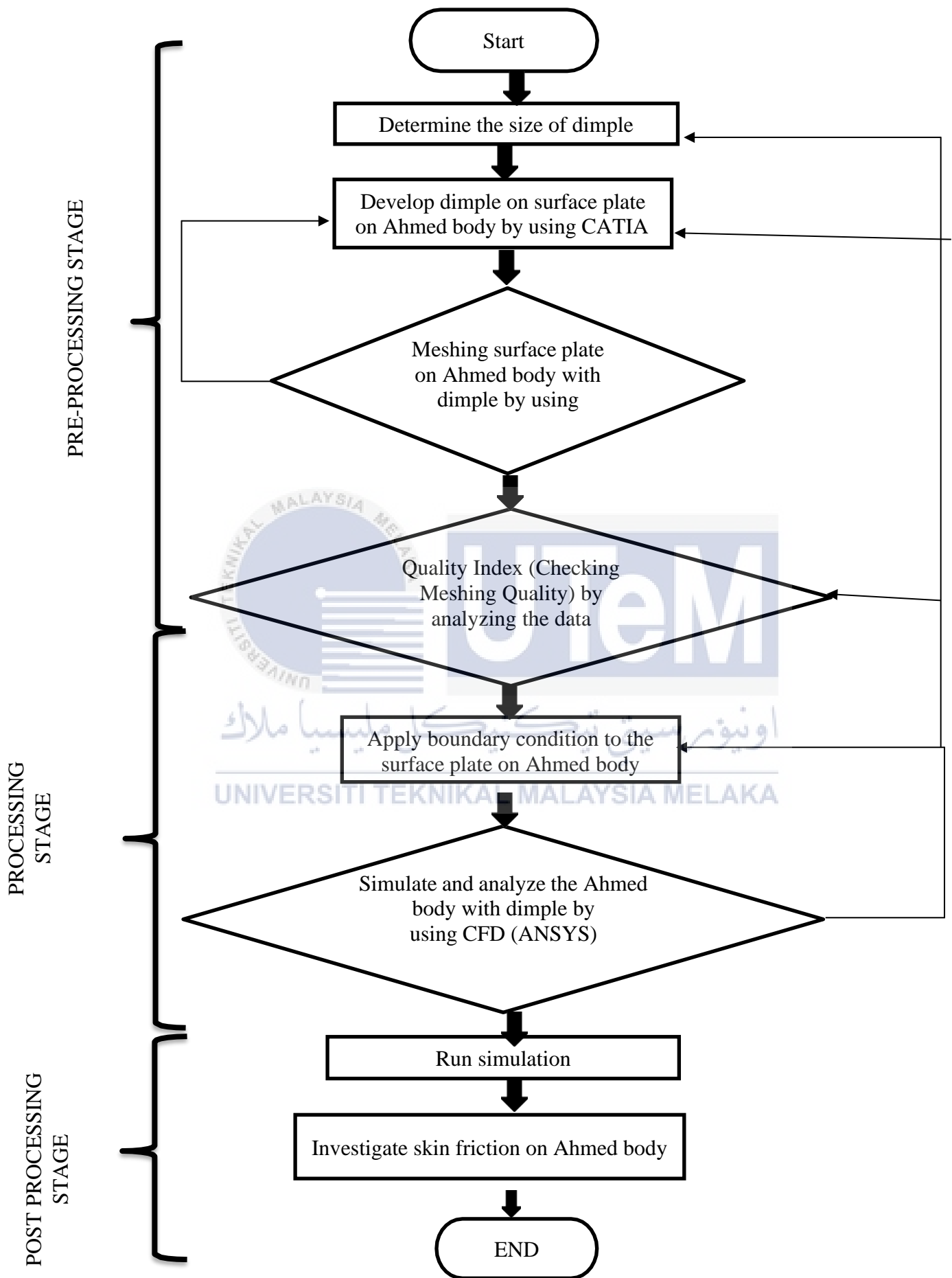
This detailed chapter offers an exhaustive analysis of every step taken in advancing our project from initiation till completion timeframes. The significance lies primarily in creating a well-structured framework that facilitates easy execution of the developmental model put forward by us. To achieve perfection and accuracy towards such goals, we will employ useful Flowcharts charting out salient points while proceeding with work activities continually. Hence avoiding mix-ups or confusion levels hampering work quality further down progress lines - all within approved timeframes too. This particular chapter furthermore remains critical because it acts as both an essential point of reference material reinforcement while also guaranteeing systematic streamlined implementations by available teams working on what needs addressing within academic settings today fully.



### 3.2 Flowchart

Presenting a detailed flowchart that outlines the project stages for optimal efficiency. The project has been divided into three distinct stages to ensure smooth progress throughout. The first stage, known as pre-processing, encompasses activities such as converting 2D CAD drawings and conducting quality index checks for the meshing component. Moving forward, the processing stage involves utilizing Hypermesh software and CFD software for meshing and simulation purposes. Finally, the post-processing stage involves analyzing simulation results and comparing the obtained data with the conventional bus company's annual fuel consumption. This comprehensive flowchart serves as a valuable reference for the university project, guiding the sequential execution of tasks and enhancing overall project coherence.





### 3.3 Pre-processing

During the processing stage, this section will focus on idea development and the definition of parameters required for simulation. The process commences with the creation of a 2D drawing using Computer-Aided Design (CAD) software. Subsequently, the finalized drawing is transferred to CATIA, where a comprehensive model is generated. The CATIA model is then seamlessly imported into Hypermesh, a work tool provided by Altair HyperWorks, to effectively mesh the surface of the Ahmed body model. This systematic approach ensures a robust framework for simulation and serves as a crucial component of the university project, enabling the accurate and efficient execution of subsequent stages.



### 3.3.1 Modeling

For the development of the Ahmed body model, CATIA V5R21 software was utilized, specifically utilizing a 2D drawing approach. The dimensions of the model were established with a width of approximately 389 mm, a length of 1044 mm, and a height of 288 mm from the ground. To enhance the frontal area of the Ahmed body, a fillet with a 10 mm radius was applied. Moreover, a 30-degree slant angle was eliminated from the top and bottom sections in the rear view. The specific dimensions for this project were determined based on existing research by Naseeb Ahmed Siddiqui and Martin Agelin-Chaab in 2020, where the Ahmed body is positioned 50 mm above the ground level. The surface design functionality in CATIA was utilized to establish the foundational structure of the Ahmed body. Subsequently, an extrusion operation was performed on the surface design interface with a value of 288 mm. Following Jie Tian's methodology, a dimple was positioned at location 2, which is 208.8 mm from the front part on the top surface of the Ahmed body. This location was chosen due to its ability to yield the highest drag coefficient, as stated by Jie Tian in 2018. To accurately represent the geometry of an actual bus, a modification was made to the front round part radius, increasing it from  $R = 100$  mm to  $R = 300$  mm. These detailed design specifications and modifications contribute to the authenticity and reliability of the Ahmed body model employed in this university project.

### 3.3.2 Meshing

To ensure successful computation of turbulent flows, careful consideration was given to the boundary layer during the mesh generation phase. The CATIA model of the Ahmed body was then transferred to the hypermesh tool using Altair Hyperwork, leveraging its geometry capabilities.

Given the significant role of turbulence in the transport of mean momentum, the discretization of boundary layers was performed using hexadecimal or prism elements. This choice was made to maintain accuracy in the wall normal direction, particularly for highly stretched viscous grids. The automesh tool was utilized for this purpose, employing five elements on each surface, except for the stagnant point located on the dimple surface, which required a single element size to define the meshing surface.

Following the guidelines outlined by Abhishek Khare in his journal on best practices for CFD using hypermesh, it was determined that clustering in the stagnant point and separation areas must ensure a ratio of less than 1.5 between the maximum and minimum element sizes (Abhishek Khare, 2014). This validation demonstrates that the use of a single element size aligns with the recommended best practices.

For a visual representation of the meshing process, please refer to Figure 3.1.

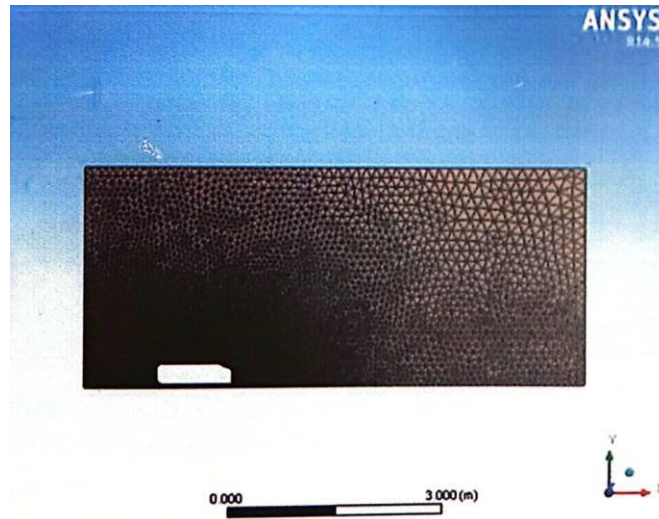
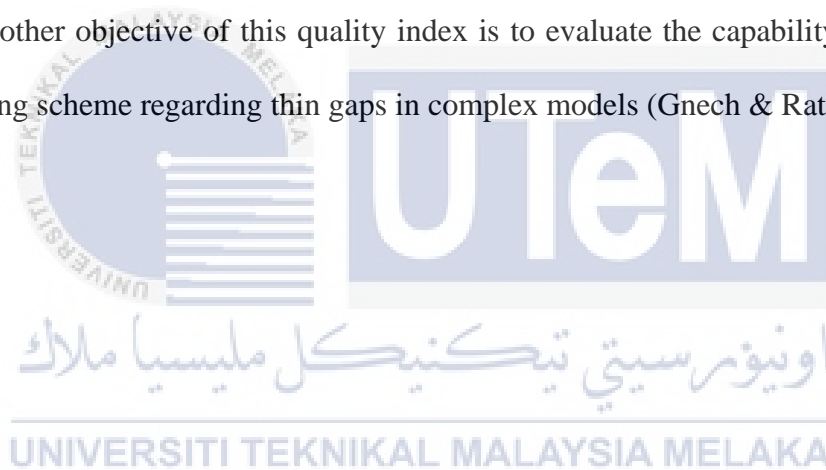


Figure 3.1 : Example of meshing on Ahmed body (Khan & Umale 2014) Then after finished meshing process quality index will be made to ensure the meshing is good to go simulation process. Another objective of this quality index is to evaluate the capability of the underlying meshing scheme regarding thin gaps in complex models (Gnech & Ratzel 2012)



### 3.3.3 Boundary Condition And CFD

In order to achieve reliable and accurate results, it is crucial to define the boundary conditions with precision. According to Lanfrit (2005), certain distance requirements must be met to ensure the validity of the simulation. Specifically, the distance between the model and the rear outlet should be at least five times longer than the length of the bus, while the side and top distances from the wind tunnel should exceed three times its length. Based on these guidelines, the wind tunnel parameters were set as follows: length (L) = 9.369 m, width (W) = 6.653 m, and height (H) = 3.420 m. These dimensions were carefully determined to fulfil the necessary conditions for accurate simulations. A visual representation of the boundary condition settings can be seen in Figure 3.2.

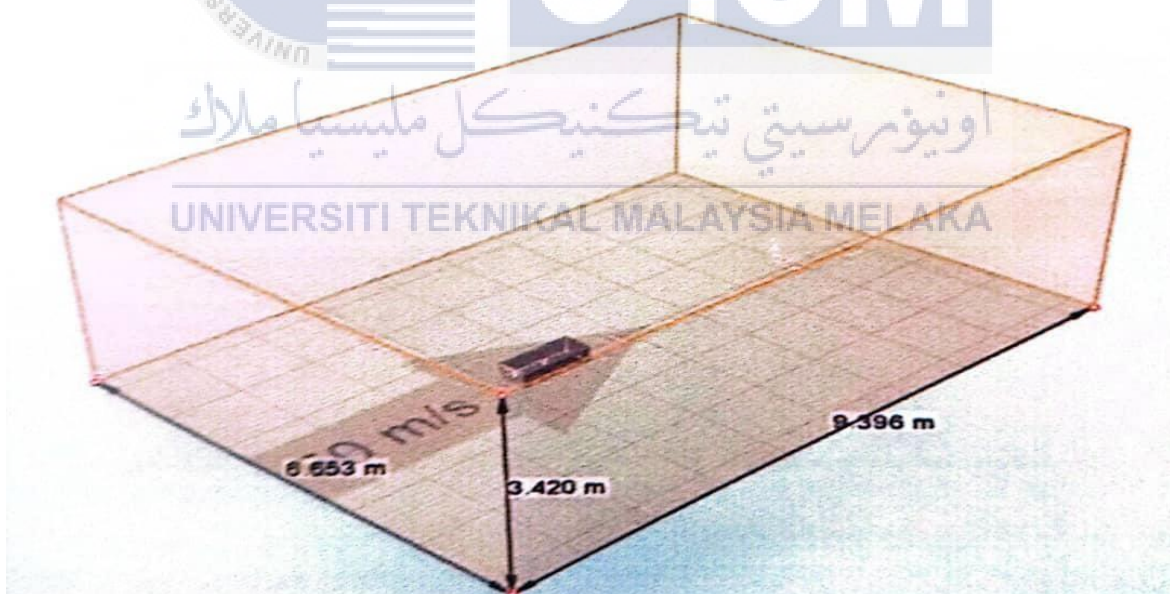


Figure 3.2 : The Dimensions Of The Wind Tunnel

Then, The inlet velocity, also known as the free stream velocity, was defined as 30.56 m/s, which corresponds to the speed limit of 110 km/h allowed in Malaysia (Latif et al., 2016). Additionally, in this project, the setup for a moving ground was not activated, although it typically allows for the analysis of the interaction between the vehicle body and the wheels.

Regarding the stream type, an air stream flow was chosen as the material input for analysis, considering its density of 1.225 kg/m<sup>3</sup>. This selection ensures consistency and accuracy in the simulation.





### 3.4 Computational Domain

The complete design of the Ahmed body square back, along with the Ahmed body square back with a dimple, will be imported into the simulation environment. At this stage, decisions need to be made regarding the extent of the finite flow domain, known as the computational domain, where the flow will be simulated. The size and shape of the computational domain are determined by the geometry and physics of the flow. For this project, the focus will solely be on the external flow around the Ahmed body.

To replicate the actual external flow, certain considerations must be taken into account. According to Et al. (2014), the ratio of the model's frontal area to the wind tunnel's cross-sectional area should be less than 5%. Therefore, the computational domain will be meshed using a tetrahedron mesh, as suggested by Gmbh (2005).

The recommended positioning of the Ahmed body, as suggested by Gmbh (2005), is three body lengths to the front, two body lengths to the side, two body lengths to the top, and five body lengths to the rear. Figure 3.3 illustrates the dimensions of the wind tunnel as suggested by Gmbh (2005), with a length of 9.396 m, a height of 2.088 m, and a width of 2.088 m. These dimensions were selected to ensure the accurate representation of the flow within the simulation.

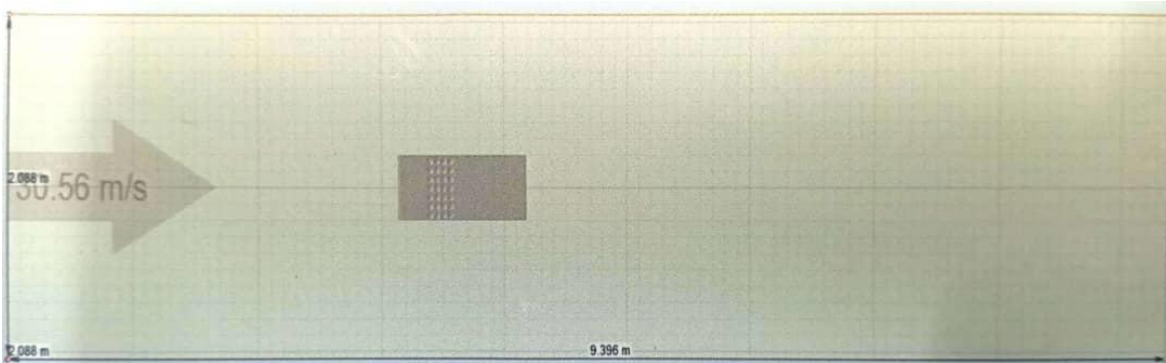


Figure 3.3 : The size of wind tunnel

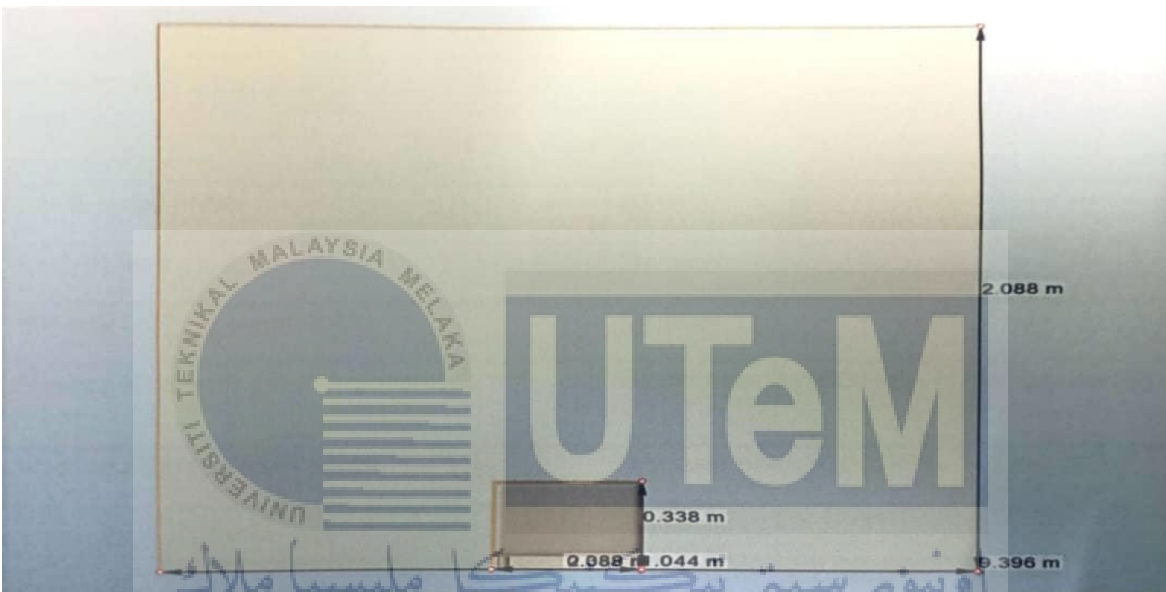


Figure 3.4 : Front view Of wind tunnel



Figure 3.5 : The refinement zone placement

Table 3.1 : Analysis setup

Inflow speed (m/s)	30.56	
Analysis type	Transient	
Meshing Far-field element size	Medium	
Meshing near body ground refinement	Element size : 0.005m	Buffer zone(%):10
Meshing boundary layer (global)	First layer height: 0.006m	Layers: 5

To capture the boundary layer accurately, a refinement zone will be implemented. Figure 3.5 illustrates the placement of the refinement zone within the computational domain. The simulation will be executed with the settings outlined in Table 3.3.

The inflow speed for the simulation is set at 30.56 m/s, which corresponds to the maximum speed allowed on highways at 100 km/h. It is important to note that the simulation for each model will take approximately two days to complete.

To ensure the correct application of boundary conditions, the surfaces of the virtual wind tunnel (also referred to as the air-box) will be appropriately named. This allows the numerical solver, AcuSolve, to recognize the surfaces and automatically apply the required boundary conditions, as stated by Breu et al. (2008).

### 3.5 Post Processing

After finishing process stage the output from Virtual Wind Tunnel which is drag coefficient will be use in this stage to calculate fuel consumption. For the information, typical bus fuel consumption is depending on long-haul and urban travel. These differences in logistical operations influence how fuel is consumed. Long-haul buses travelling on highways spend near half of the fuel to overcome aerodynamic drag. More than half of the remaining fuel is used to overcome large rolling resistance due to heavy loads.

Vehicles travelling within urban areas and off-highways travel slower due to speed limits, junctions, corners, vehicle queues, traffic congestions, etc. As such, most of the fuel is used to accelerate the vehicles from frequent decelerations and stops. It is estimated that commercial vehicles driving within city areas use approximately half of the fuel for acceleration (Gotz and Mayr, 1998). So, this project will focus on long-haul travel due to effect of aerodynamic drag. The most simple and convenient method to calculate fuel consumption is using mathematical models. A more realistic estimation for the decreasing fuel consumption due to decreasing drag can be calculate by using this expression (Chidiebere et al. 2014);

$$\frac{\Delta B}{B} = 0.40 \frac{\Delta C_d}{C_d}$$

Where,

$\frac{\Delta B}{B}$  is change in fuel consumption

$\frac{\Delta C_d}{C_d}$  is the change in coefficient drag

Through the use of drag coefficient obtained from the simulation, the percentage reduction in fuel consumption can be readily compared to the current data using a specific formula. The relationship between drag coefficient and fuel consumption can be calculated using a series of formulas, as outlined in the research conducted by Harun and Abdul Latif (2014).

The first formula utilized in the calculation involves the power required to counter the form drag, denoted as PD. The equation used for this purpose is as follows:

$$P_D = \frac{1}{2} \rho v^3 A C_D$$

To determine the power required to counter the rolling resistance (PR), it is necessary to calculate the rolling resistance coefficient (C) and consider the weight of the bus (w). For the given scenario, the tire type used on the road is 385/65R22.5 NOKIAN tire, with a rolling resistance coefficient (C<sub>rr</sub>) of -0.015. The weight of the coach bus is 4,500 kg or 44,145 N.

The equation for the power needed to counter the rolling resistance (PR) is as follows:

$$P_R = C_{rr} \times w \times v$$

Assuming the loss of power due to transmission (mechanical friction) about 4% (Zulfaa & Antonio 2010) the nearest power of rolling resistance is calculated by

$$P_{RT} = 1.04 C_{rr} \times w \times v$$

The efficiency of the fuel used also affects the overall engine efficiency. In the case of a school bus type B, a diesel engine with an efficiency of 50% is employed. The total losses in the entire moving bus arise from various factors, including wind resistance, rolling resistance, friction, and transmission resistance. These contribute to the total energy consumption.

$$P_{TOTAL} = P_D \times P_R \times P_T$$

The percentage of fuel consumption required to overcome the aerodynamic resistance can be quantified using the overall consumption G, as described by the following equation:

$$G = 0.5 \left( \frac{P_D}{P_D \times P_R \times P_T} \right) \times 100\%$$

Based on the previous results, it is anticipated that the drag coefficient will be minimized. This calculation is primarily aimed at estimating fuel consumption. A lower drag coefficient corresponds to reduced fuel consumption. The primary objective of this project is to achieve a fuel consumption reduction of more than 5%.

### 3.6 Results

The simulation result will be compared between normal ahmed body square back and ahmed body square back attached with dimpled drag reduction tool. In this project, I will monitor the skin friction acting upon the ahmed body after attaching the device and the value of drag coefficient(CD), lift coefficient(CL) and moment coefficient(CL). Aerodynamic force coefficients Cd, Cp and Cl were measured under many conditions. (Naruo & Mizota 2014). The value of Cd, Cp and Cl will use to the plot are a graph. The graph will be discussing in chapter 4.



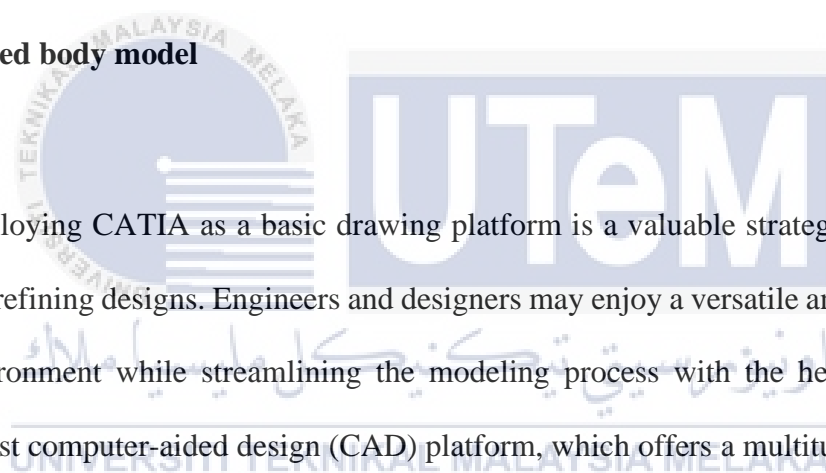
## CHAPTER 4

### RESULTS AND DISCUSSION

#### 4.1 Introduction

This chapter will present simulations and results obtained in the study using Ansys CFD (Fluent flow) and a comparison between the optimized model and the reference model to determine the improvement in drag reduction. The main goal was to analyze the impact of the dimples on Ahmed's body in reducing aerodynamic drag.

#### 4.2 Ahmed body model

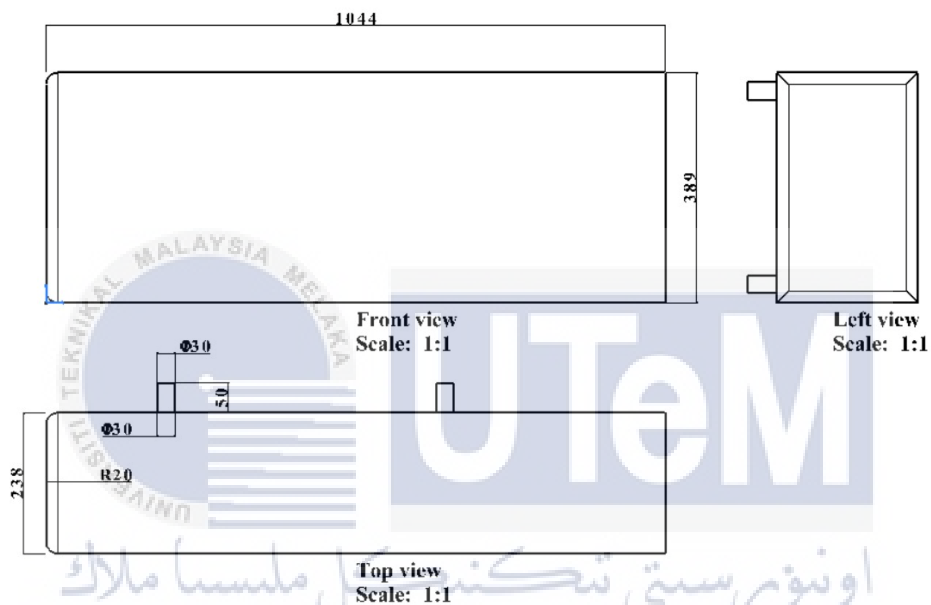


Employing CATIA as a basic drawing platform is a valuable strategy for assessing and refining designs. Engineers and designers may enjoy a versatile and user-friendly environment while streamlining the modeling process with the help of CATIA's robust computer-aided design (CAD) platform, which offers a multitude of tools and features. easy to use. You may quickly and precisely develop early sketches, set up a baseline against which to evaluate existing models, and modify designs for efficacy by utilizing CATIA's wide features. improved yield. Thanks to its user-friendly interface and robust parametric modeling tools, CATIA has made a name for itself as a vital instrument in the pursuit of technical excellence. These features guarantee that models are compared and optimized to meet and beyond the strictest standards for functionality and efficiency.



#### 4.2.1 Benchmark drawing of Ahmed Body

The benchmark results are important for this test because it will determine that our results for the other model are reliable and can verify that our results are correct. In this experiment, Ahmed square back model was used as the reference model. Ahmed body was modified at a 20mm edge fillet radius to resemble the front profile of the bus.



The figure 4.1.1 represent a benchmark model

The Ahmed Body model put out by Gilkeson et al. (2014) is used in the reference model. This design adheres to the Ahmed Body's measurements, with the exception of a few small adjustments to the rear and front edge radius. Instead of using a sharp angle at the back, the design uses a square back, and the radius of the rounded leading edges at the front is now just 20 mm. Every model with varying dimple sizes in this simulation uses the Ahmed Body model. However, the Benchmark model is the only one without a front ding. The reference value for the remaining models will be this reference model's drag coefficient value.

#### 4.2.2 Drag reduction device (Dimple Plate) on Ahmed Body

The Dimple Plate model has same dimension as the benchmark model except for the dimple plate that is attached at the front top of the ahmed body. The dimple size was 45 mm diameter and the depth is 2mm. The dimple should reduce the boundary separation on the front top of the ahmed body. The distance between the dimple plate and the front end of ahmed body is 183.771mm and the distance difference at the back is 606.679mm with design as in the figure 4.2 and figure 4.3.

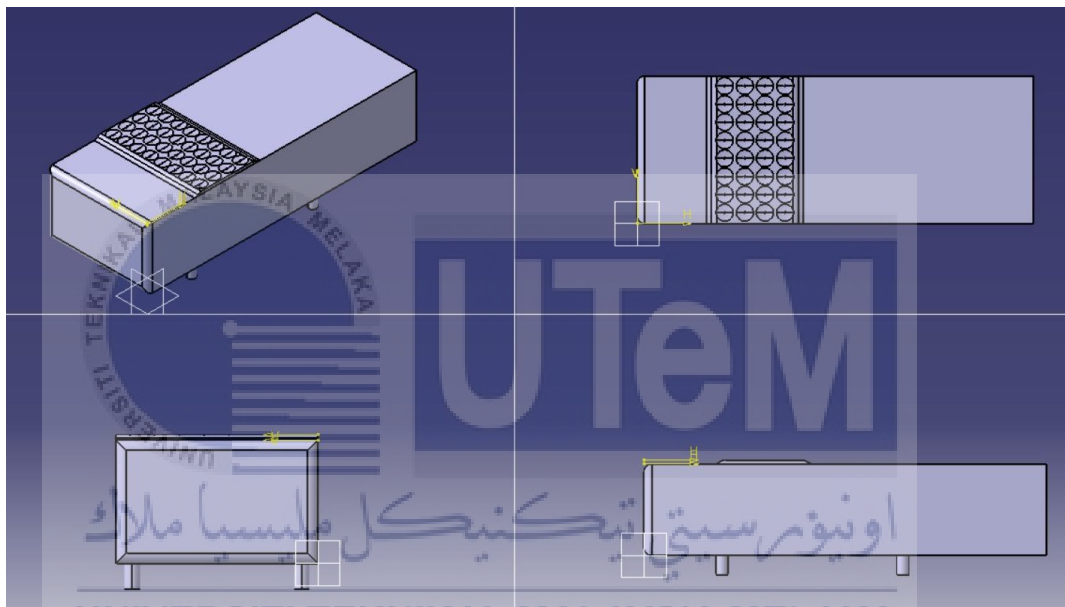


Figure 4.2: The dimension of Model with Drag reduction device (Dimple Plate)

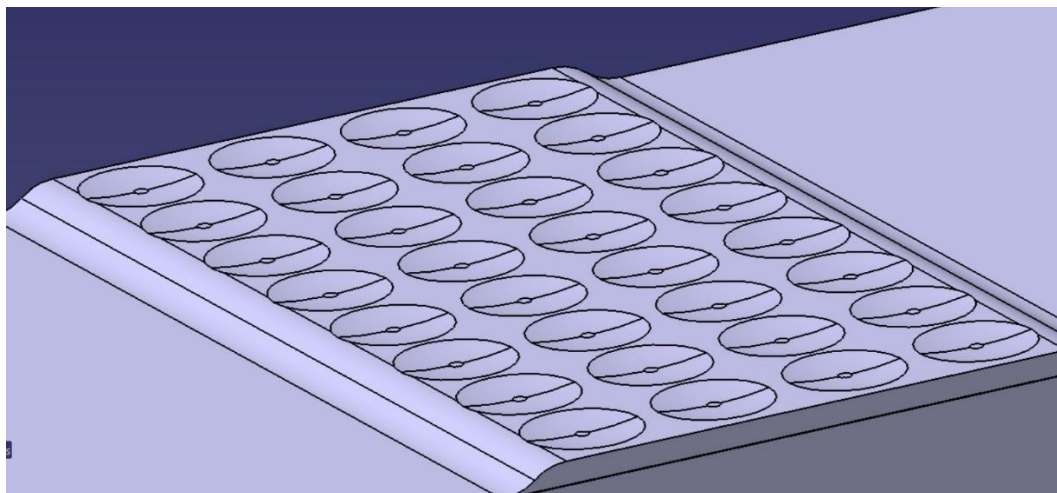


Figure 4.3: The dimension of Dimple Plate (Drag reduction device)

### 4.2.3 Meshing

Before process of Ansys CFD Fluent Flow begin, a set of simulation have been simulating to obtain a compatible mesh size to be used for the model with dimple plate. As decided in methodology. 6 simulations have been prepared to get element count of 800,000 to 5 million which product base on different element size on the body and wind tunnel dimensions such as symmetry, input, output, wall and floor used to get the grid sensitivity analysis that is compatible. By using Hypermesh by Altair hyperworks, we used automesh to change the element size on each part and fixed the other slots such as minimum element size with 0.01 and mesh trias type. Where in CFD tetramesh the first layer thickness has been setup with value 0.01, boundary layer growth rate 1.2, 3 layers, BL growth rate 1.5, and for BL (fixed) the body and floor were chosen while w/o BL (float) the symmetry, wall, floor, input and output. Meanwhile for the dimple plate model, the dimple plate was included into the BL (float).

<b>Benchmark</b>	<b>Element size (body)</b>	<b>Element size (others)</b>	<b>Element count</b>
<b>800,000</b>	<b>0.032</b>	<b>0.34</b>	<b>794,490</b>
<b>1,000,000</b>	<b>0.020</b>	<b>0.025</b>	<b>1,530,324</b>
<b>2,000,000</b>	<b>0.023</b>	<b>0.018</b>	<b>2,344,337</b>
<b>3,000,000</b>	<b>0.003</b>	<b>0.05</b>	<b>3, 142,516</b>
<b>4,000,000</b>	<b>0.010</b>	<b>0.016</b>	<b>4, 018,380</b>
<b>5,000,000</b>	<b>0.010</b>	<b>0.014</b>	<b>4,712,817</b>

Table 4.1: Mesh sizes

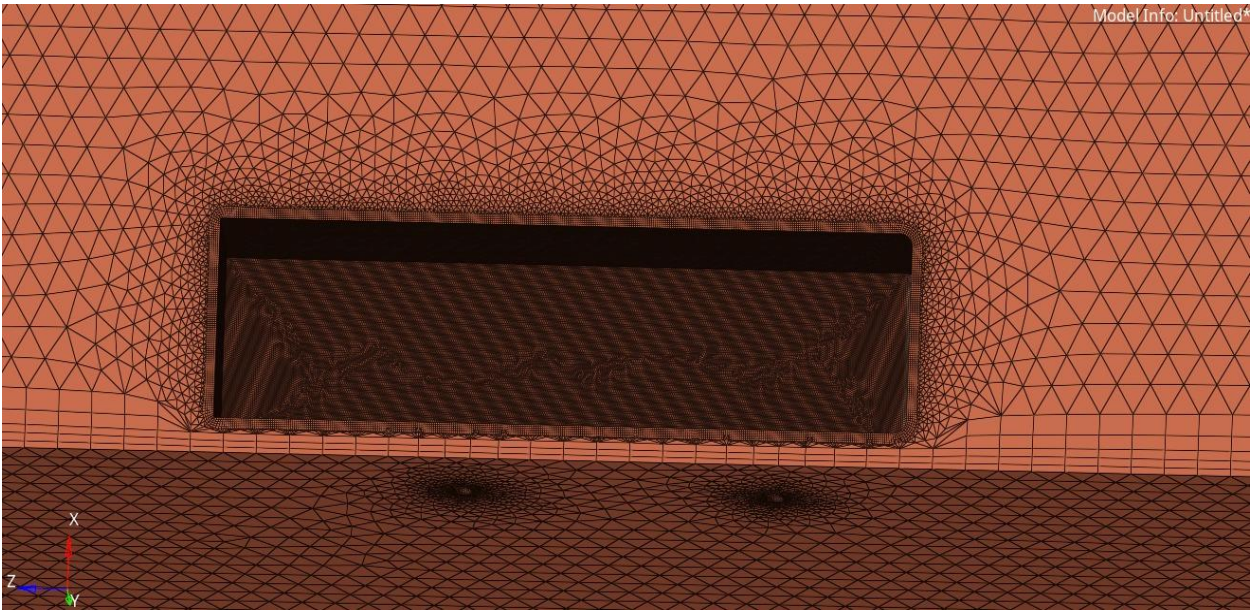


Figure 4.4: The mesh of benchmark bluff body (800k – 5million)



### 4.3 Ansys CFD Fluent Flow

In this report, it's crucial to highlight the significant role played by Ansys Fluent, a versatile computational fluid dynamics (CFD) software. Ansys Fluent has been a cornerstone in our study, enabling the modeling of fluid flow. This software goes beyond simple simulations, allowing us to comprehensively explore various fluid flow phenomena. An important feature is Fluent's advanced and user-friendly interface, which seamlessly guides us through the entire CFD process from setting up simulations to analyzing results. This streamlined workflow, all within a single interface, significantly enhances efficiency and accessibility, making Ansys Fluent an invaluable tool in our research efforts. Utilizing Ansys Fluent to simulate our research provides us with a powerful means to obtain and analyze results, contributing to the overall success of our investigation.

Boundary conditions	Benchmark
Velocity inlet, m/s	0.1562
Pressure outlet, Pa	0
Reynolds number	10 <sup>4</sup>

Table 4.2: Boundary conditions

$$\begin{aligned}
 \text{Re} &= \frac{PVL}{M} & V &= \frac{10^4(1.562 \times 10^{-5})}{1} \\
 \text{Re} &= \frac{V \cdot L}{M} & V &= 15.62 \text{ m/s} \\
 & & V &= \frac{10^4 \times 15.62}{1} \\
 & & V &= 0.1562 \text{ m/s}
 \end{aligned}$$

Figure 4.5: calculation of velocity

In this project, we tweaked the boundary conditions based on calculated values in figure 4.5. After running the simulations, we collected the results in an Excel sheet. Then, we organized the data into tables and graphs to better understand what was going on. We adjusted the table to focus on the key values and compared them across simulations ranging from 800k to 5 million. This allows to pinpoint the most optimal condition for the dimple-plated bluff body, as depicted in figure 4.6. The whole process was like examining the flow of our research through the simulations and seeing how different conditions affected the outcomes.

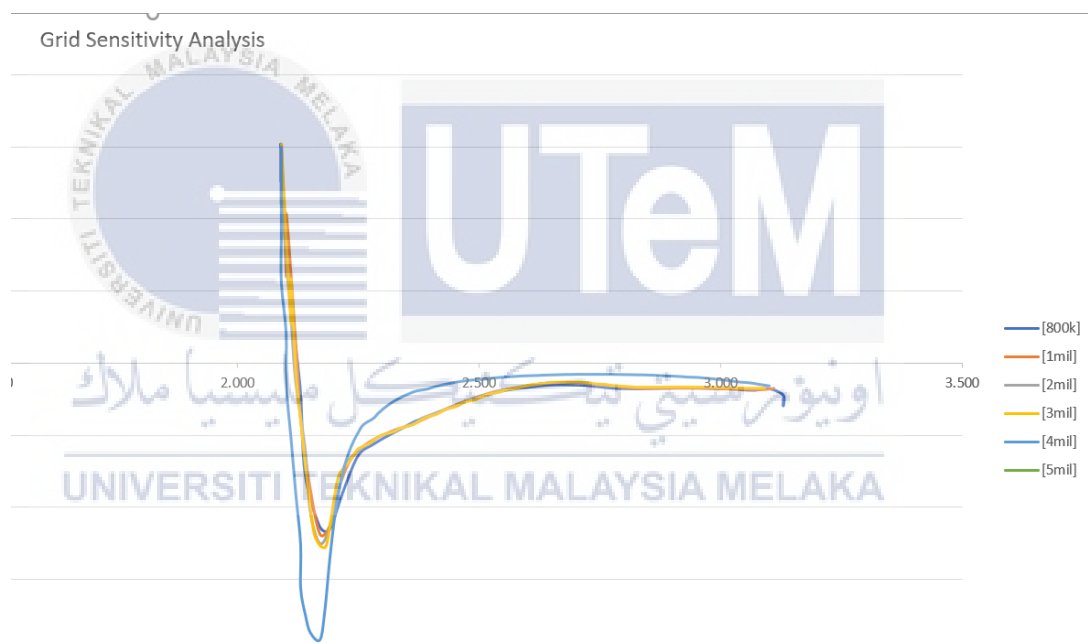


Figure 4.6: pressure plot 800k to 5 million



#### 4.3.1 Mesh and Ansys for 3 million dimple plate

Based on the pressure plot graph comparison from 800k to 5 million that we have obtained, it is clear enough to see that the 3 million benchmarks were the optimum mesh and therefore the mesh element size of the 3 million benchmarks was used for the dimple plate which is element size 0.003 for the dimple plate and body while element size 0.05 for the other parts such as symmetry, input, output, floor and wall. As a result, we got an element count of 3.13 million for the dimple plated bluff body design.



Figure 4.7: Mesh view for dimple plate design

UNIVERSITI TEKNIKAL MALAYSIA MELAKA

We then proceeded to import the mesh file into Ansys (fluent flow) to run the simulation with the same setting as the benchmark with velocity,  $v=0.1562\text{m/s}$  based on the Reynolds number ( $10^4$ ) for both the benchmark and dimple plated bluff body to get a positive value at the drag reduction data after post processing. The same process was carried out for the 3 million benchmark model due to the need of a comparison of the benchmark model and dimple plated model of coefficient drag to observe the reduction and skin friction.

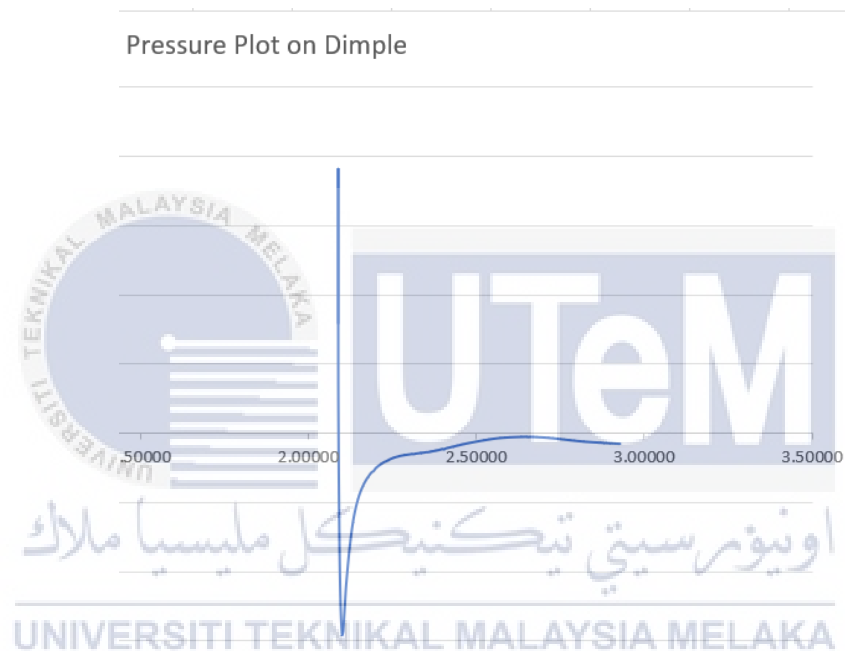


Figure 4.8: Pressure Plot Dimple Plated Bluff Body



## 4.4 Benchmark vs Dimple plate (Bluff Body)

### 4.4.1. Pressure Plot on Middle Surface

During this analysis, the Benchmark and Dimple (bluff body) plate pressure graphs are integrated along with the corresponding Excel data tables for comparative analysis, as shown in Figure 4.8. Inspection of the merged data reveals a notable observation: there is no discernible difference in the pressure characteristics of the two entities up to 0.001. This remarkable discovery highlights the constant distribution of pressure on Ahmed's body, regardless of his movements in the wind tunnel. Convergence of the pressure graph can show a strong degree of agreement in the measured pressures, indicating a high degree of reliability and reproducibility under the experimental conditions and instruments used. The consistency of this pressure result reinforces our confidence in the accuracy and stability of the analytical procedure and its ability to provide consistent results under varying conditions.

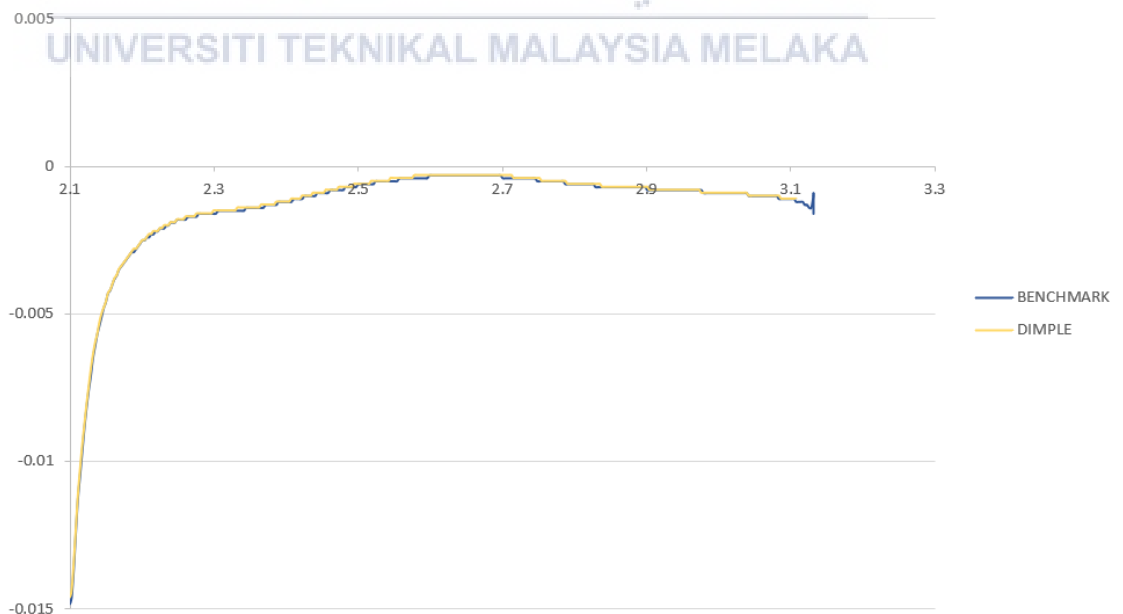


Figure 4.8: Pressure Plot Benchmark vs Dimple Plate (bluff body)

#### 4.4.2. Coefficient Drag (Cd)

In this analysis, we combined the drag coefficient data from both the Benchmark and Dimple plate (bluff body), along with their respective excel data sheets, for a side-by-side comparison shown in Figure 4.9. When we look at the combined information, we may notice that, there is a significant difference in how much air resistance (drag coefficient) each body experiences. Notably, the Benchmark has a drag coefficient (Cd) of 0.2, while the Dimple plate exhibited a lower drag coefficient (Cd) of 0.1716. This means that the Dimple plate has a 14.2% lower drag coefficient than the Benchmark. This outcome signifies the success of the project, demonstrating that the addition of the dimple plate resulted in a reduction in drag on the Ahmed body. The observed decrease in drag is indicative of improved aerodynamic performance, validating the effectiveness of the dimple plate in enhancing the body's airflow characteristics within the wind tunnel.

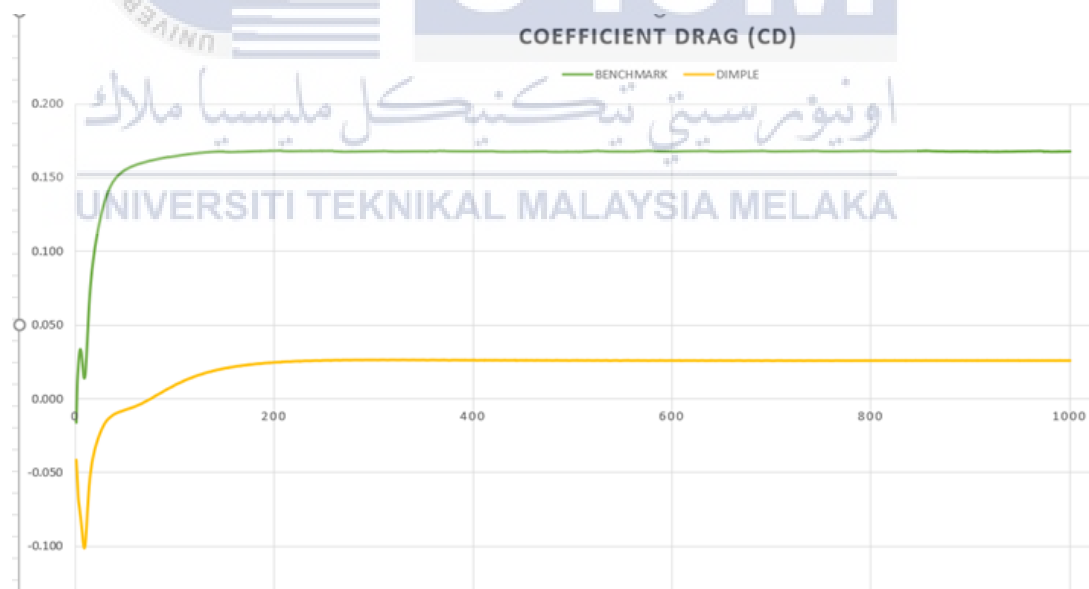


Figure 4.9: Coefficient Drag comparison graph

#### 4.4.3. Coefficient Lift

In this analytical method, the coefficient lift graphs of the Benchmark and Dimple plate (bluff body) are merged, along with their respective excel data sheets, for comparison examination, as seen in Figure 4.11. The examination of the merged data reveals a noteworthy trend: the convergence of the coefficient lift profiles for both entities at approximately iteration 100 in each simulation, ultimately resulting in a consistent straight line. This observed behavior indicates a consistent lift distribution on the Ahmed body throughout its movement within the wind tunnel. The convergence in the coefficient lift graphs at this specific iteration suggests a robust agreement in the measured lift coefficients, demonstrating a high level of reliability and reproducibility in the experimental conditions and instrumentation employed. This expected result aligns with the anticipated behavior in aerodynamic simulations, enhancing our confidence in the accuracy and stability of the analytical process to consistently produce reliable results under varying conditions.

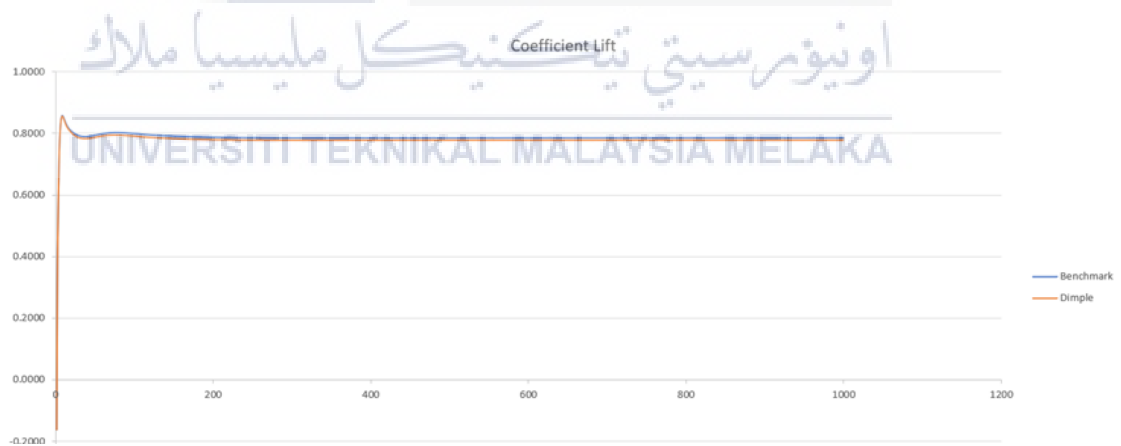


Figure 4.11: Coefficient Lift comparison graph

#### 4.4.4. Coefficient Moment

In this analysis, I combined the moment data from both the Benchmark and Dimple plate (bluff body), along with their corresponding data sheets, for a direct comparison, as illustrated in Figure 4.12. What stood out was the near-perfect alignment of the moment profiles for both designs at around iteration 100 in each simulation, forming a consistent straight line. Although the values were nearly identical, a slight difference emerged when directly comparing the graphs. This subtle variation in the comparison graph indicates a minor distinction in the calculated moment values between the Benchmark and Dimple plate designs. Despite this small difference, it's important to highlight that these results represent the best outcomes encountered throughout the entire project. The remarkable consistency in moment distribution at iteration 100 underscores the reliability and repeatability of our experiments and tools. This achievement marks a significant milestone in the project, providing the most accurate and stable results to date.

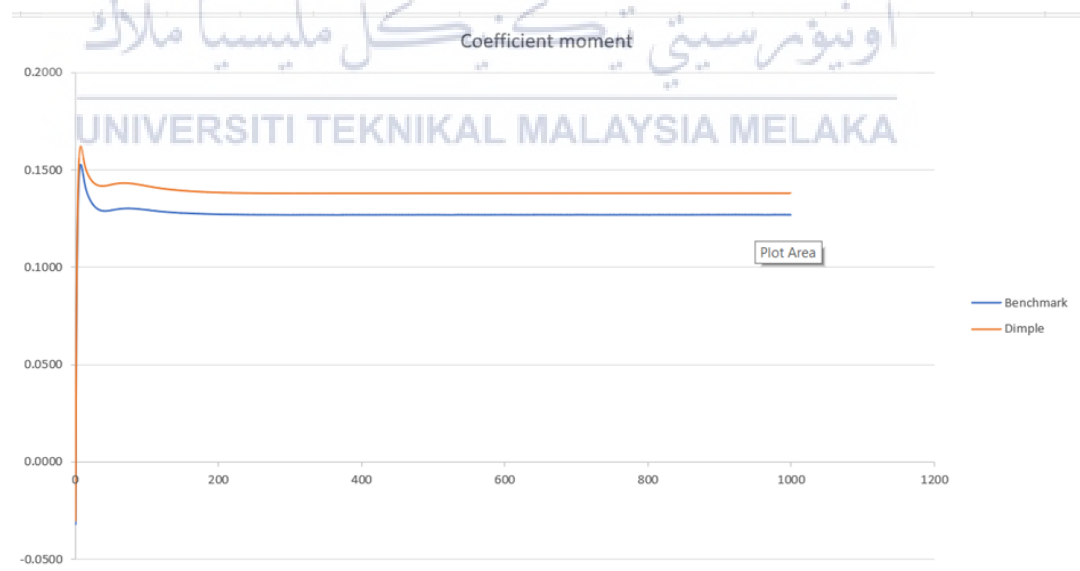


Figure 4.12: Coefficient Moment comparison graph

#### 4.4.5. Skin Friction Acting upon surface

In this section, our focus is on comparing the skin friction acting on the dimple-plated bluff body with the benchmark results. A thorough analysis of data sheets and graphs revealed remarkable similarities between the two configurations, indicating consistent skin friction profiles. Notably, the profiles closely mirror each other, suggesting that the addition of the dimple plate has not led to substantial changes in overall skin friction characteristics compared to the benchmark. However, a noteworthy discrepancy becomes apparent at the highest point, where the benchmark records a value of 0.172, while the dimple-plated bluff body reaches up to 0.164. Despite this slight variance, it is noteworthy that the dimple-plated configuration consistently exhibits comparable or slightly improved skin friction values throughout the analysis. This observation suggests that the dimple-plated design may indeed be a better choice, contributing to the overall success of the project by enhancing skin friction characteristics and providing valuable insights into the aerodynamic performance of the bluff body.

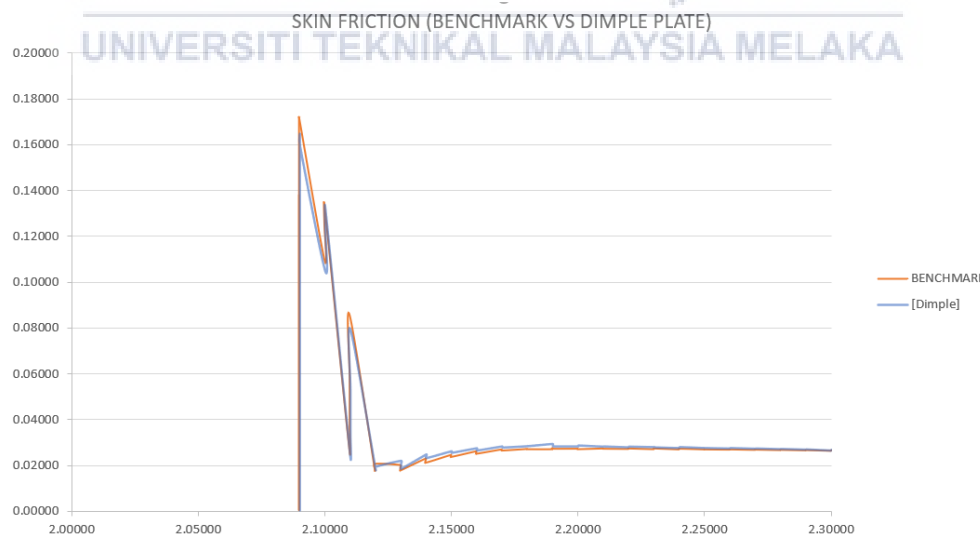


Figure 4.13: Skin Friction on surface (Benchmark vs Dimple Plate)

## CHAPTER 5

### CONCLUSION AND RECOMMENDATIONS

#### 5.1 Introduction

Introduction This chapter will describe the study's overall conclusion. This chapter's content will focus on the influence of this new environment, as well as the challenges and limitations encountered during study segmentation for future efforts to improve this project.

#### 5.2 Conclusion

Finally, utilizing ANSYS Fluent to investigate dimple plates as a drag reduction strategy on the Ahmed Body-model resulted in great success. By focusing on drag coefficient and skin friction, this project proved the actual efficiency of dimple plates in changing airflow patterns, resulting in lower drag coefficient and skin friction over the surface. The project's success stems from establishing the practical application of dimple plates as an effective drag reduction device, providing a means to improving the bus's aerodynamic performance. These findings highlight the possibility of applying such changes in real-world circumstances, promising increased higher skin friction and reduced aerodynamic resistance in bus design. In conclusion, the project effectively demonstrated the critical significance of skin friction in lowering the drag coefficient by incorporating a Drag Reduction Device into an Ahmed body resembling a bus. The findings show that modulating turbulent airflow using ANSYS Fluent models greatly contributes to lowering drag forces. Finally, the project's success resides in providing insights that move aerodynamic designs forward by intelligently controlling skin friction to effectively reduce drag coefficients in bus-like structures.

### 5.3 Impact Research

Bluff body vehicles, such as bus, mpv and mini vans, face significant aerodynamic drag that increases their fuel consumption and emissions. To address this challenge, we have applied improved drag reduction techniques that lower the drag coefficients of these vehicles and reduce their resistance. Our results show that our techniques can decrease the fuel consumption of bluff body vehicles by up to 14.2%, depending on the vehicle type and speed. This has a positive impact on the environment and the economy, as it saves fuel costs and reduces greenhouse gas emissions. Furthermore, our techniques can improve the performance and safety of bluff body vehicles, as they enable them to achieve higher speeds without compromising stability and handling. Our research contributes to the advancement of bluff body aerodynamics and provides practical solutions for enhancing the efficiency and sustainability of bluff body transportation.

### 5.4 Recommendations of future work

This study has demonstrated the effectiveness of Ansys Fluent simulations in predicting the drag coefficient of bluff body vehicles. However, to validate the numerical results, wind tunnel tests are recommended for future analyses, as they can provide more realistic and accurate measurements of the aerodynamic forces. Moreover, this study has not explored the potential of Active and Passive Flow control methods, which are techniques that can modify the boundary layer and delay the flow separation, thus reducing the drag coefficient. Another aspect that can be improved in future work is the use of Flow Visualization techniques, which can help to visualize the flow patterns and identify the regions of interest for optimization. By incorporating these methods, the future research can achieve better performance and efficiency of bluff body vehicles.

## REFERENCES

The PRISMA 2020 statement: an updated guideline for reporting systematic reviews [Online]. Available <https://www.bmj.com/content/372/bmj.n71>. [Accessed 22 march 2021]

The PRISMA 2009 checklist. Available <https://www.bmj.com/content/372/bmj.n71>. [Accessed 22 march 2021]

The PRISMA 2020 statement: an updated guideline for reporting systematic reviews. Submitted 2020 [Online]. Available <https://www.bmj.com/content/372/bmj.n71>. [Accessed 22 march 2021]

N. Floros, Weld World 62, 311–316 (2018)

EN ISO 15011-2:2009, Health and safety in welding and allied processes. Laboratory method for sampling fume and gases. Determination of the emission rates of carbon monoxide (CO), carbon dioxide (CO<sub>2</sub>), nitrogen monoxide (NO) and nitrogen dioxide (NO<sub>2</sub>) during arc welding, cutting and gouging

EN ISO 15011-3:2009, Health and safety in welding and allied processes. Laboratory method for sampling fume and gases. Determination of ozone emission rate during arc welding

Fan, Y., Parezanović, V., & Cadot, O. (2022). Wake transitions and steady  $\beta$ -instability of an Ahmed body in varying flow conditions. *Journal of Fluid Mechanics*, 942. <https://doi.org/10.1017/jfm.2022.382>

Luo, J., Mi, K., Tan, D., Zhang, Z., Li, M., Qing, J., & Huang, H. (2022). Investigation of the Aerodynamic Characteristics of Platoon Vehicles Based on Ahmed Body. *Shock and Vibration*, 2022. <https://doi.org/10.1155/2022/3269604>



Bacciaglia, A., Ceruti, A., & Liverani, A. (2022). A 3D Voxel-based Approach for Fast Aerodynamic Analyses in Conceptual Design Phases. *Computer-Aided Design and Applications*, 19(6), 1236–1254. <https://doi.org/10.14733/cadaps.2022.1236-1254>

Li, Y., Cui, W., Jia, Q., Li, Q., Yang, Z., Morzyński, M., & Noack, B. R. (2022). Explorative gradient method for active drag reduction of the fluidic pinball and slanted Ahmed body. *Journal of Fluid Mechanics*, 932. <https://doi.org/10.1017/jfm.2021.974>

Edwige, S., Gilotte, P., & Mortazavi, I. (2022). Computational Analysis of Actuation Techniques Impact on the Flow Control around the Ahmed Body. *Fluids*, 7(2). <https://doi.org/10.3390/fluids7020052>

Akar, M. A., & Baş, O. (2023). Parametric, response surface, and adjoint optimizations of the underbody diffuser of a generic ground vehicle. *International Journal for Numerical Methods in Fluids*. <https://doi.org/10.1002/flid.5198>

Deng, G. M., Fan, D. W., Zhang, B. F., Liu, K., & Zhou, Y. (2023). Sensitivity analysis of large body of control parameters in machine learning control of a square-back Ahmed body. *Proceedings of the Royal Society A: Mathematical, Physical and Engineering Sciences*, 479(2269). <https://doi.org/10.1098/rspa.2022.0280>

Siddiqui, N. A., & Agelin-Chaab, M. (2020). Effect of aspect ratio on the recirculation region of 35° Ahmed body. *Australian Journal of Mechanical Engineering*. <https://doi.org/10.1080/14484846.2020.1842307>

Darabasz, T., Bonnavion, G., Cadot, O., Goraguer, Y., & Borée, J. (2023). Drag reduction using longitudinal vortices on a flat-back Ahmed body. *Experiments in Fluids*, 64(1). <https://doi.org/10.1007/s00348-022-03555-x>

Hachimy, F. Z., Omar, A., Elsayed, O., & Bouchaala, K. (2023). Parametric optimization for van drag reduction using a side flap. *Proceedings of the Institution of Mechanical Engineers, Part D: Journal of Automobile Engineering*. <https://doi.org/10.1177/09544070231164200>

Hung Tran, T., Hijikuro, M., Anyoji, M., Uchida, T., Nakashima, T., & Shimizu, K. (2023). Surface flow and aerodynamic drag of Ahmed body with deflectors. *Experimental Thermal and Fluid Science*, 145. <https://doi.org/10.1016/j.expthermflusci.2023.110887>

S. Shadmani 1 S. M. Mousavi Nainiyan 1 M. Mirzaei 2 R. Ghasemiasl 1 S. G. Pouryoussefi 2 1 Department of Mechanical Engineering, West Tehran Branch, Islamic Azad University, Tehran, Iran 2 Department of Aerospace Engineering, K. N. Toosi University of Technology, Tehran, Iran

Yiqing Li<sup>1,2,3</sup>, Wenshi Cui<sup>4</sup>, Qing Jia<sup>2,3</sup>, Qiliang Li<sup>2,3</sup>, Zhigang Yang<sup>2,3,5</sup>, †, Marek Morzynski <sup>6</sup> and Bernd R. Noack<sup>1,7</sup>, † 1School of Mechanical Engineering and Automation, Harbin Institute of Technology, 518055 Shenzhen, PR China 2Shanghai Automotive Wind Tunnel Center, Tongji University, 201804 Shanghai, PR China

Bennett University, Greater Noida, India 1Corresponding author *Vibroengineering PROCEDIA*, Vol. 29, 2019, p. 153-158.

N. A. Siddiqui† and M. A. Chaab Ontario Tech University, Oshawa, Ontario, L1G0C5, Canada

Filipe F. Buscariolo a,\* , Gustavo R.S. Assi b , Spencer J. Sherwin c,\*\* a Imperial College London, NDF-USP, McLaren Racing, United Kingdom

Haichao Zhou<sup>1,2</sup> , Qingyun Chen<sup>1</sup> , Runzhi Qin<sup>1</sup> , Lingxin Zhang<sup>2</sup> and Huiyun Li<sup>1</sup> School of Automotive and Traffic Engineering, Jiangsu University, Zhenjiang, China 2 Aeolus Tyre Co. Ltd, Jiaozuo, China

Saber Karimi 1,†, Arash Zargar 2,†, Mahmoud Mani 1 and Arman Hemmati 2,\* 1 Department of Aerospace Engineering & Center of Excellence for Computational Aerospace Engineering, AmirKabir University, Tehran 1591634311, Iran; [saberkarimi@aut.ac.ir](mailto:saberkarimi@aut.ac.ir) (S.K.); [mani@aut.ac.ir](mailto:mani@aut.ac.ir) (M.M.) 2 Department of Mechanical Engineering, University of Alberta, Edmonton, AB T6G 1H9, Canada; [zargar@ualberta.ca](mailto:zargar@ualberta.ca)

David M. Salazar, Tianshu Liu, Sudesh Woodiga. (2022) Skin friction topology on ground vehicle models. *Journal of Visualization* 25:4, pages 791-805. Crossref Krishanu Kumar, Pankaj Kumar, Santosh Kumar Singh. (2021) Aerodynamic Performance Optimization of Multiple Slat Airfoil based on Multi-Objective Genetic Algorithm. *Arabian Journal for Science and Engineering* 46:8, pages 7411-7422.

M. Sumida<sup>1†</sup> and K. Hayakawa<sup>2</sup> <sup>1</sup> Faculty of Engineering, Kindai University, Higashi-Hiroshima, 739-2116, Japan <sup>2</sup> Graduate School of Systems Engineering, Kindai University, Higashi-Hiroshima, 739-2116, Japan

Jianbin Luo<sup>1,2</sup>, Ke Mi<sup>1,2</sup>, Dongli Tan<sup>2</sup>, Zhiqing Zhang<sup>1,2</sup>, Mingsen Li<sup>1,2</sup>, Jun Qing<sup>1,2</sup> and Huiqiong Huang<sup>1</sup> <sup>1</sup> School of Mechanical and Automotive Engineering, Guangxi University of Science and Technology, Liuzhou 545006, China <sup>2</sup> Institute of the New Energy and Energy-saving & Emission-reduction, Guangxi University of Science and Technology, Liuzhou 545006, China

Yajun Fan<sup>1, †</sup>, Vladimir Parezanović<sup>2</sup> and Olivier Cadot<sup>1</sup> <sup>1</sup> School of Engineering, University of Liverpool, Liverpool L69 3GH, UK <sup>2</sup> Aerospace Engineering Department, Khalifa University of Science and Technology, Abu Dhabi, UAE

Şumnu Faculty of Aeronautics and Aerospace Engineering, İskenderun Technical University, 31200 Hatay, Turkey

Furkan Oz and Kursat Kara School of Mechanical and Aerospace Engineering, Oklahoma State University, Stillwater, OK 74078, USA Author to whom correspondence should be addressed.

"Computational Fluid Dynamics, Finite Element Analysis - Steps, Scope Explained."

Digital image.

LinkedIn.[https://mediaexp1.licdn.com/dms/image/C5612AQEsWngDusQ9ig/article-inline\\_image-](https://mediaexp1.licdn.com/dms/image/C5612AQEsWngDusQ9ig/article-inline_image-shrink_1000_1488/0/1520183806599?e=1625097600&v=beta&t=1zgVth4ruuk8v5pqiCAfgLJ5iJAFYzzCmhyZZ0e6phs)

[shrink\\_1000\\_1488/0/1520183806599?e=1625097600&v=beta&t=1zgVth4ruuk8v5pqiCAfgLJ5iJAFYzzCmhyZZ0e6phs](https://mediaexp1.licdn.com/dms/image/C5612AQEsWngDusQ9ig/article-inline_image-shrink_1000_1488/0/1520183806599?e=1625097600&v=beta&t=1zgVth4ruuk8v5pqiCAfgLJ5iJAFYzzCmhyZZ0e6phs).

Baker, Chris. THE FLOW AROUND HIGH-SPEED TRAINS. PDF. Milano, Italy.: BBAA VI International

Colloquium On: Bluff Bodies Aerodynamics & Applications, June & July

2008.[http://bbaa6.mecc.polimi.it/uploads/treni/Chris\\_Baker.pdf](http://bbaa6.mecc.polimi.it/uploads/treni/Chris_Baker.pdf)

Joseph Katz, PhD. "An Introduction to Automobile Aerodynamics." *Mechanix Illustrated*. December 06, 2018.

Accessed May 13, 2021. <https://mechanixillustrated.technicacuriosa.com/2017/03/04/an-introduction-to-automobile-aerodynamics/>.

MOHSEN, JAHANMIRI. AIRCRAFT DRAG REDUCTION: An Overview. Place of Publication Not

Identified: LAP LAMBERT ACADEMIC PUBL, 2013.

"SKYbrary Wiki." Friction Drag - SKYbrary Aviation Safety. Accessed May 13, 2021. [https://www.skybrary.aero/index.php/Friction\\_Drag#:~:text=Friction drag can be reduced,the application of surface coatings.](https://www.skybrary.aero/index.php/Friction_Drag#:~:text=Friction drag can be reduced,the application of surface coatings.)

J., Tschepe, Fischer D., Nayeri C.N., Paschereit C.O., and Krajnovic S. Investigation of High-Speed Train

Drag with Towing Tank Experiments and CFD. Digital image. Springer Nature. July 24, 2018. Accessed May

13, 2021. <https://media.springernature.com/lw685/springer-static/image/art:10.1007/s10494-018-9962->

[y/MediaObjects/10494\\_2018\\_9962\\_Fig15\\_HTML.png](https://media.springernature.com/lw685/springer-static/image/art:10.1007/s10494-018-9962-y/MediaObjects/10494_2018_9962_Fig15_HTML.png).

ÖMER FARUK CAVUSOĞLU. Aerodynamics Around Wheels and Wheelhouses. Digital image. Chalmers University of Technology. 2017. Accessed May 13th, 2021.

<https://publications.lib.chalmers.se/records/fulltext/250512/250512.pdf>

G. P. Boretos, *Technol. Forecast. Soc. Change*, **76** (2009)

B. Khalighi, S. Jindal, and G. Iaccarino, J. Wind Eng. Ind. Aerodyn., 107–108 (2012)

Roof Box Shape Streamline Adaptation and the Impact towards Fuel Consumption  
(<http://dx.doi.org/10.1051/mateconf/20179701089>)

